in the Horner term and BHT respectively. The distinction between dependent and independent error is an important one and is necessary in the x direction as the uncertainty in this term is derived from both t_C and t_L (Appendix 4). Whilst each given data point is possessed of an individual t_L, all data points within the same well must be characterised by the same t_C. Were this not the case then the well would be in violation of one of the basic model conditions and could not be used. The consequence of this condition is that, whilst error due to t_L may fluctuate independently from point to point, error due to t_C may not.

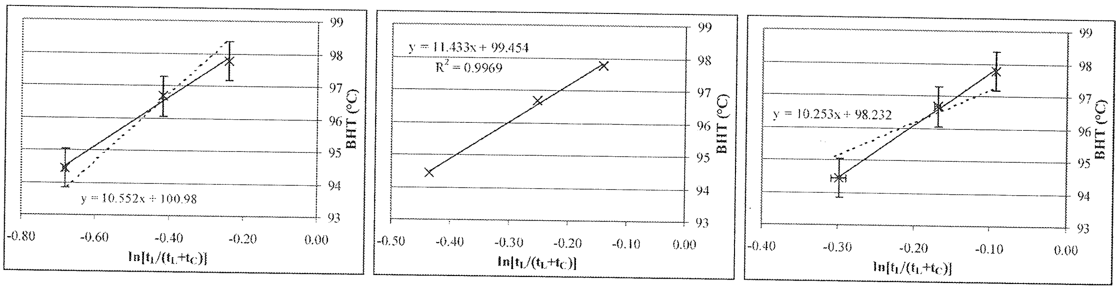

Figure 5.5: Error envelope determined for a typical three-point Horner regression in well Taloola 2. The central graph represents the best-fit Horner solution as shown in Figure 5.1. To the left is the upper limit of uncertainty, to the right the lower limit of uncertainty. The solid regression lines in the LHS and RHS graphs represents the outer limits of regression defined by the dependent uncertainty in estimated t_C, which is constant for each regression. Error bars superimposed upon these lines indicate the independent uncertainty on each point due to the resolution limits of t_L and BHT. The dotted regression lines indicate the maximum (left) and minimum (right) possible predictions of T_{eq} calculated when the total variation due to both dependent and independent errors is taken into account. Equations for these lines are shown for comparison with the actual result. As before, the y-intercept indicates the magnitude of predicted T_{eq}. Please note: the error envelope has been depicted in this way so as to enable the relatively small x-error bars to be visible.

It should be clear from Figure 5.5 that the total calculated uncertainty in the Horner term $[\ln(t_L/(t_L + t_C)]$ can be quite large (Appendix 4). Such large errors in input data should, on face value, translate to correspondingly large uncertainty in the temperature prediction. This is not the case for the Horner plot however as the majority of uncertainty in the x-term is sourced from the calculation of t_C. As t_C must be held constant for each point the range of valid regression lines is restricted, drastically reducing the number of ways in which a straight line may be fitted to the data. The possible range of intercept values is thus constrained by the model conditions and the uncertainty in predicted T_{eq} is reduced. Thus, despite uncertainties in t_C that are typically in excess of ±50% the error in predicted temperature due to this uncertainty is usually less than ±1%. For the 57 wells included in this analysis, the mean uncertainty in predicted T_{eq} due to variation in t_C was only +0.9 and –0.8°C.

Compared to the magnitude of the percentage error in t_C, the uncertainty from primary input parameters t_L (x) and BHT (y), visible as error bars in Figure 5.5, seems relatively minor, encompassing only a small range of possible values for each data point. Unlike the error in t_C however, the value of these uncertainties may vary from point to point, allowing a relatively large range of possible gradients for the regression line. Determination of the possible range of uncertainty in predicted T_{eq} produced as a result of the superposition of these errors on top of those already determined for t_C was a relatively simple graphical exercise for the majority of wells, which have only three data points (Figure 5.5). The average total uncertainty in predicted T_{eq} so determined from these wells (total 48) was +2.1% and -1.8% (+2.6°C and -2.2°C). This value is over double that caused by the uncertainty in t_C alone implying that the bulk of systematic uncertainty in the prediction of T_{eq} is, rather ironically, derived from the least uncertain input parameters. Were the variations in t_L or BHT to be of equivalent size (in percentage terms) as those of t_C, the effects on model prediction accuracy would likely be dramatic.

Combining the total determined uncertainty in the Horner predicted T_{eq} with that determined for the SLEX temperatures (Chapter 4; Appendix 4) gives an uncertainty in prediction accuracy of –2.6; +2.2%. For the SLEX temperatures this implies a mean overall prediction accuracy range of between -2 and –7%, confirming the bias in the model. For FTEX temperatures the equivalent range of uncertainty is likely to be larger although for reasons outlined in Chapter 4 this is difficult to quantify.

5.7 Sensitivity Analysis

It is clear from the above results that, for CBST wells, the Horner model on average forecasts static temperatures that are lower than the true formation temperature. To understand why this may be so, and to guard against possible bias arising from otherwise unaccounted influences, it is necessary to examine the model response with respect to a number of variables. These include both input parameters and a variety of other factors already identified in Chapter 4 which have the potential to influence model results. Should model results be found to fluctuate in a systematic way with one or more variables then the parameters in question may be used in a predictive way, either to rule data out of consideration or, perhaps more significantly, to forecast the size of the bias expected in the model result.

Factors identified in Chapter 4 as having potential to influence model results include the CBL reliability (category), the presence of coal bearing formations between the CBL and BHT depth, the number of pre-logging conditioning episodes, the type (shape) of the temperature-time curve and the number of available data points. Box plots of Horner prediction accuracy relative to the FTEX split along these lines are provided in Figures 5.6 . Also included in this figure is a plot of prediction accuracy split between statistically significant and non-significant regressions. Scatter graphs of prediction accuracy versus input parameters including initial t_L, total length t_L, total lag window, total t_C and the ratio (initial)t_L/t_C are presented in Figure 5.7 as well as those for CBL extrapolation distance, CBL lag time, and model fit (R^2).

Examining first the box plots, it is apparent that, overall, individual result populations are relatively uniform with no major outlier(s). SLEX and FTEX results appear relatively consistent, although the greater overall range of the former is apparent. Bearing in mind the limitations produced by large variations in population size it does appear that, on average, the quality of prediction is slightly improved in wells with four rather than three data points, type 1 curve shapes, category 2 CBL, only one episode of pre-logging well conditioning, no coal between the CBL and BHT depth and/or statistically significant regressions (although it has already been established in this last case that this distinction cannot be resolved at 95% confidence). Examination of the available data reveals strong commonality between the population of statistically significant regressions and those of 4 point and type 1 curves (Figure 5.8). In other words, the shape and length of the data curve is exercising a strong influence on the success of the regression.

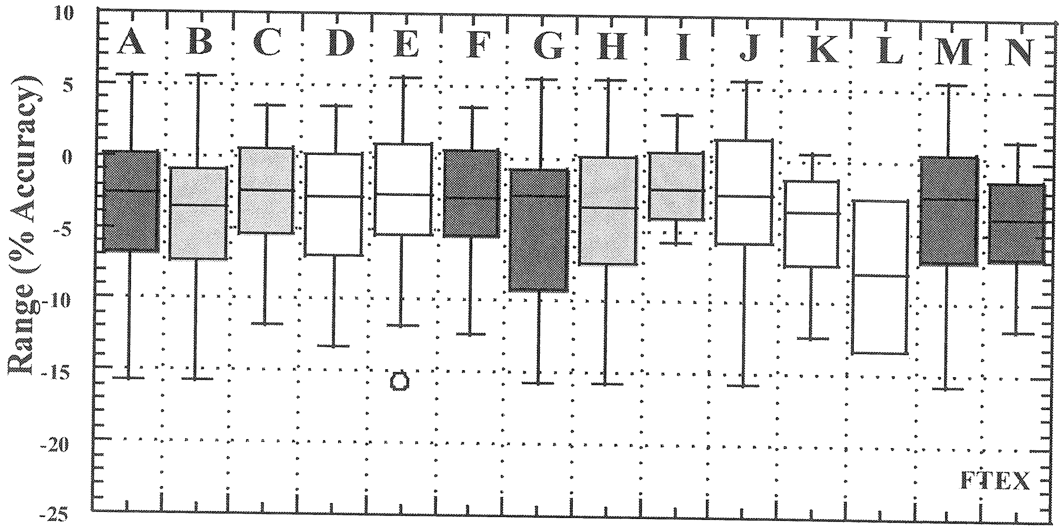

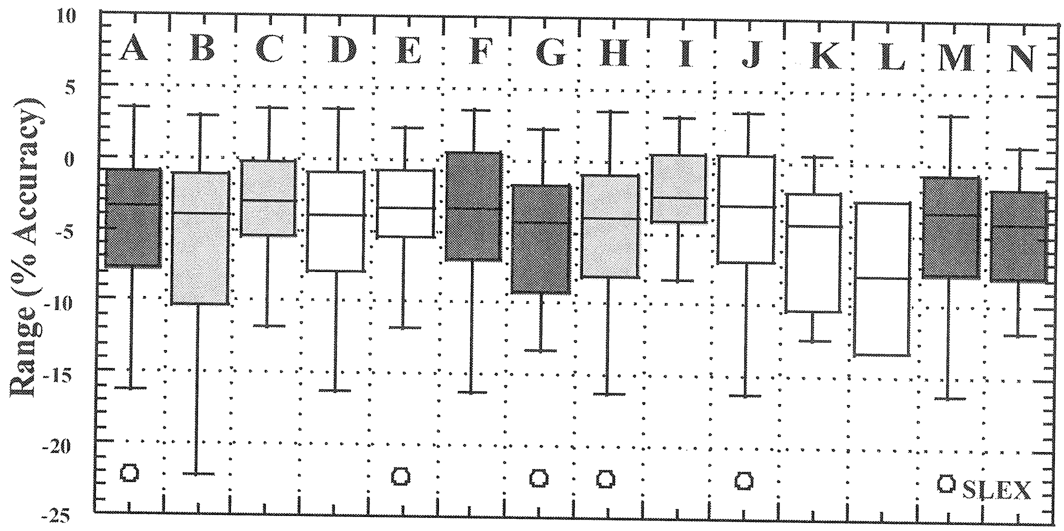

Figure 5.6: Box plots showing population distribution of results of Horner Plot formation temperature prediction accuracy relative to FTEX (top) and SLEX (bottom) static temperatures. (**A**) total population (n = 57); (**B**) subset of wells with statistically non-significant regressions (failure of regression F-test; n = 27); (**C**) subset of wells with statistically significant regressions (n = 30); (**D**) subset of wells with CBL category 1 (n = 46); (**E**) subset of wells with CBL category 2 (n = 11); (**F**) subset of wells with no coal bearing formations between CBL and BHT depth (n = 38); (**G**) subset of wells with coal bearing formations between CBL and BHT depth (n = 19); (**H**) subset of wells with three BHT data points only (n = 48); (**I**) subset of wells with four or more BHT data points (n = 9); (**J**) subset of wells with type 1 curves (n = 43); (**K**) subset of wells with type 2 curves (n = 12); (**L**) subset of wells with type 3 curves (n = 2); (**M**) subset of wells with only one recorded pre-logging conditioning episode (n = 49); (**N**) subset of wells with two or more recorded pre-logging conditioning episodes (n = 8).

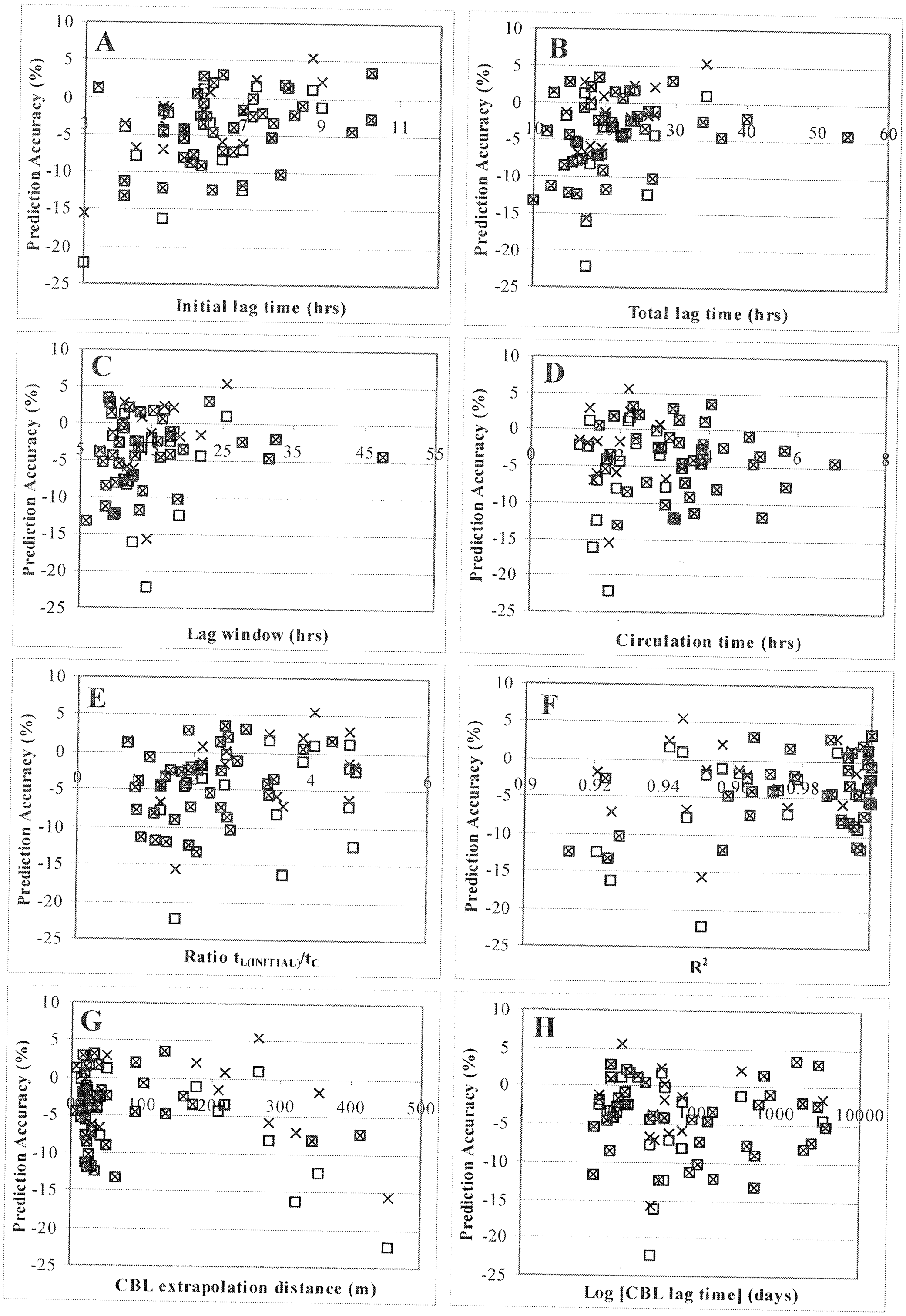

Figure 5.7: Scatter graphs depicting the accuracy of Horner Plot formation temperature prediction as percentage difference from estimated SLEX (squares) and FTEX (crosses) static temperature for 57 CBST wells versus (**A**) initial BHT lag time; (**B**) final BHT lag time (total lag time); (**C**) lag window (final – initial lag times); (**D**) total circulation time; (**E**) the ratio of initial lag time to total circulation time; (**F**) model fit (R^2); (**G**) the extrapolation distance of the CBL temperature and (**H**) the CBL lag time.

From the previous statistical analysis it is apparent that some factor must be influencing the success or failure of the model prediction in such a way that a good model fit can generate an under-predicted result. What this factor might be is not immediately obvious from the box plots in Figure 5.6. Whilst some bias may be introduced by the use of category (2) CBL temperatures the effect of these data is actually to shift prediction accuracy toward over-prediction. This is significant as it implies that these temperatures are probably slightly lower than true formation temperature and are certainly not affected by thermal anomalies produced by the hydration of casing cement. That the category (2) CBL data should display a slight temperature depression is consistent with the reduction of recovery time prior to measurement and suggests that the strongest influence on these temperatures is the drilling thermal effect. The lack of a discernable relation between prediction accuracy and CBL lag time is further supported by the scatter graph (H) included in Figure 5.7 which shows no discernable correlation.

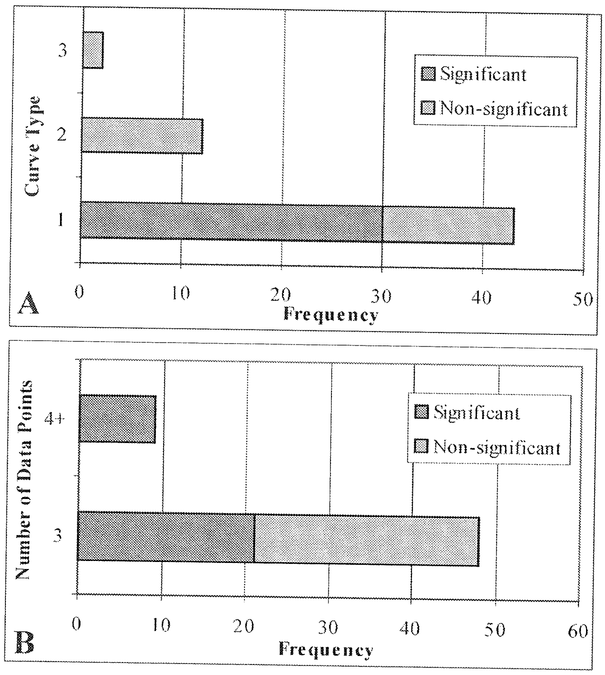

Figure 5.8: Bar graphs illustrating the relationship between the statistical significance of Horner Plot model regression and (A) curve type; (B) number of available data points.

The presence of coal bearing formations between CBL and BHT depth should bias the extrapolated static temperature toward a lower-than-actual value and hence favour over-predicted model temperatures. In fact, from the boxplot data, the opposite appears to be true implying that the presence of coal may not be of great significance to the final result. By contrast, the negative bias observed in cases where wells have been subject to multiple pre-logging conditioning may have a real physical cause. This is most probably related to an underestimation of the true circulation time. The total number of these wells is only eight however and the range of under-prediction in this population is not sufficient to account for the bias in the population as a whole.

The real clue as to what may be causing chronic model under-prediction actually lies in the apparent improvement of prediction accuracy in wells with four or more data points. The key to the success of these data is not the reduction of statistical error that comes with an extra data-point but rather the increase in the sampled window of lag time that results from the addition of an extra logging run. Examining the scatter graphs of Figure 5.7 it is evident that, in spite of a large scatter, a visible correlation exists between the accuracy of the predicted result and the length of lag time, t_L. That there should be such a relationship is not surprising given the conclusions of Chapter 3. It is clear from theory (Figure 3.3) that the failure of the Horner solution at short lag times implies that even an excellent model fit will necessarily produce a static temperature under-prediction in cases where t_L is too low. This theory closely matches the pattern of Horner prediction in Cooper Basin wells evident in Figure 5.7 where initial t_L of less than around 7 hours produce results with increasingly strong negative bias and the relation between R^2 and prediction accuracy is weak. By contrast, inital t_L greater than 7 hours produce, with one main exception (Woolkina 2), an apparently unbiased result close to ±5% of the true value. Similarly, and also with exception of Woolkina 2, it is possible to observe an overall increase in FTEX prediction quality to around ±5% in wells where the lag window is >15 hours and/or total t_L is >20 hours. For SLEX data results are similar but with the addition of a further outlying data point in the form of well Ulandi 2.

Viewed in this light it is obvious that wells with four or more data points, which naturally have longer data windows, should produce more accurate temperature predictions. Likewise, well defined Type 1 curves, which are also found to be characterised by greater mean lag window and total lag time than Type 2 or Type 3 curves, also tend to produce more accurate results. The apparent improvement of model prediction in statistically significant regressions may thus be tied to physical conditions, as those wells with four data points and/or Type 1 curve shape typically produce a good model fit and hence a successful regression. The failure of the model at short lag times however implies that successful regression alone, whilst producing a more precise result, does not necessarily produce a more accurate one. These results will be discussed further in Chapter 9.

CHAPTER 6

TESTING THE DMZC MODEL OF COOPER & JONES (1959)

6.1 Introduction

Unlike many other models for BHT correction the method of Cooper & Jones (1959) (hereafter C&J) appears to have experienced relatively little attention in the forty years since its creation. Whilst most other model forms, including line source and constant temperature DMFC, have been regularly revisited and developed, the DMZC model seems to have been largely ignored. Given this apparent neglect, it was perhaps a little surprising when the comparative study of eleven BHT correction methods carried out by Hermanrud *et al.* (1990; Table 3.1) concluded that this method was the most accurate (but not the most precise) of all models studied.

An explanation for the apparent neglect of the DMZC approach is likely to be found in the inherent complexity of the function upon which it relies. Analytical solution of $F(\alpha, \tau)$ is possible but requires Laplace transformation. Several authors, including Bullard (1954), Jaeger (1956) and Davis (1988), provide tabulated solutions for the function enabling approximation either by interpolation or rounding of known inputs. Neither of these methods is completely satisfactory however and in the absence of modern computing power it seems the model may have been considered too difficult for everyday use and was thus effectively shelved. Fortunately this situation has now changed and the function may be quickly and easily approximated via application of Simpson's Rule. In the present case approximate solutions for $F(\alpha, \tau)$ were generated using the technique of Beardsmore & Cull (2001) adapted into a new VBA macro **F_alpha_tau** (Appendix 5). Use of this protocol facilitated the rapid calculation of a large number of results, important when dealing with a database the size of the CBST.

6.2 Input Parameters

Unlike the Horner method, the DMZC model for borehole thermal re-equilibration described by C&J disregards circulation time (t_C) and is thus spared the problems associated with the estimation of this parameter. The assumption of dual media, however, does require quantative knowledge of the thermal properties of both the formation and the well contents (mud). In all, six parameters are necessary in addition to t_L and BHT: well radius a, mud density ρ_m, mud specific heat c_m, formation density ρ_f, formation specific heat c_f, and formation thermal conductivity k_f. Estimation of these parameters, and their associated uncertainties, has already been described in Chapter 4.

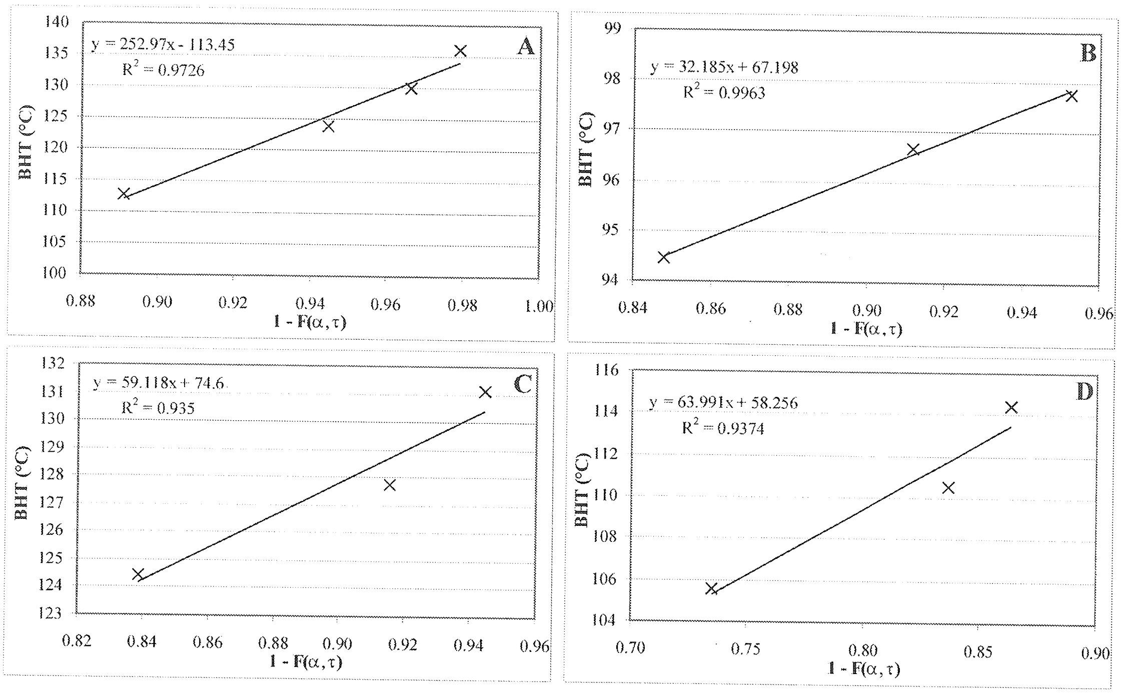

Figure 6.1: Typical examples of DMZC model regression. Predicted equilibrium temperature is given by the sum of the gradient and the y-intercept. (A) Bookabourdie 2 (SLEX = 144.3); (B) Taloola 2 (SLEX = 104.2); (C) Woolkina 2 (SLEX = 148.8) and (D) Della 10 (SLEX = 138.1). Refer to Figure 4.6 for comparison with the primary temperature-time data curves.

6.3 Application of the DMZC Model

Following the calculation of F(α, τ) described above, solution of the DMZC model for BHT temperature correction was a relatively simple graphical process and was undertaken within Microsoft Excel. Examples of the graphical results produced by the application of the DMZC method to selected CBST wells are presented in Figure

6.1. For the purposes of comparison, the wells sampled here are the same as those in Figures 4.6 and 5.1.

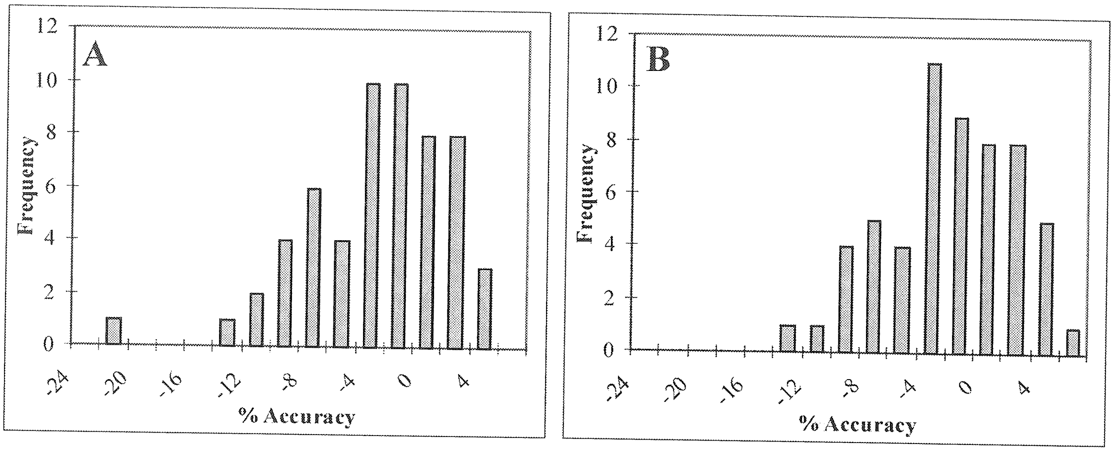

Figure 6.2: Results of DMZC model formation temperature prediction from fifty-seven (57) CBST wells. Accuracy is calculated relative to the known static formation temperature, positive numbers indicate percentage over-prediction, negative percentage under-prediction. In graph (**A**) static temperatures are all straight line extrapolated (SLEX), in (**B**) formation compensated static temperatures (FTEX) are used where available.

6.4 Model Results

The overall fit of well data to the model curve appears to be quite good with only four wells characterised by $R^2 < 0.90$. Perhaps not coincidentally these were the same four wells which were excluded from use in the Horner model - the extreme Type 3 curve of Spencer 5, the fast recovery curve of Burke 1, the problematic, high t_C/low t_L Brumby 4 and the type 2 curve of Big Lake 32. Exclusion of these four wells increases the overall average R^2 from 0.9619 to 0.9763.

Histograms and standard descriptive statistics of the static temperature prediction accuracy of results generated by the C&J method are presented in Figure 6.2 and Table 6.1.

	SLEX	FTEX
Mean	-4.6	-3.7
Standard Error	0.7	0.6
Median	-4.0	-3.4
Standard Deviation	5.1	4.7
Sample Variance	26.3	22.2
Kurtosis	1.2	-0.3
Skewness	-0.9	-0.4
Range	25.7	21.0
Minimum	-22.0	-15.5
Maximum	3.6	5.5
Count	57.0	57.0
Confidence Level (95.0%)	1.4	1.3

Table 6.1: Standard descriptive statistics for the histogram distributions of DMZC model results as given in Figure 6.2.

The distribution of predicted static temperature generated from the DMZC cylindrical source model is remarkably similar to that of the Horner plot. An overall bias toward under-prediction is evident in the mean, the predicted T_{eq} on average 4.6% less than the SLEX static temperatures and 3.7% less than the FTEX. As for the Horner data, the magnitude of the mean under-prediction is reduced when results are compared to the FTEX static temperatures. The range of prediction accuracy is generally large, equal to 25.7 for the SLEX and 21.0 for the FTEX. Standard deviation is reduced from 5.1 in the SLEX to 4.7 in the FTEX. Using the method of Tabachnich & Fidell (1996) the SLEX distribution is again found to be characterised by a significant skew to the left. Probability plots of both the SLEX and FTEX result population confirm this skew in the former, while the latter does not appear to deviate significantly from a normal distribution (Figure 6.3).

6.5 Statistical Analysis

Of the fifty-seven available C&J regressions only thirty pass the regression F-test at $\alpha = 0.05$ and may be considered to be statistically significant. This subset includes all wells with four or more data points and those wells with three data points for which $R^2 > 0.9931$. Average R^2 of the thirty significant regressions is 0.9894, that of the twenty-seven non-significant regressions 0.9618. Once again there is a strong correlation with the results of the Horner model, all but two of the thirty significant regression wells common to both models.

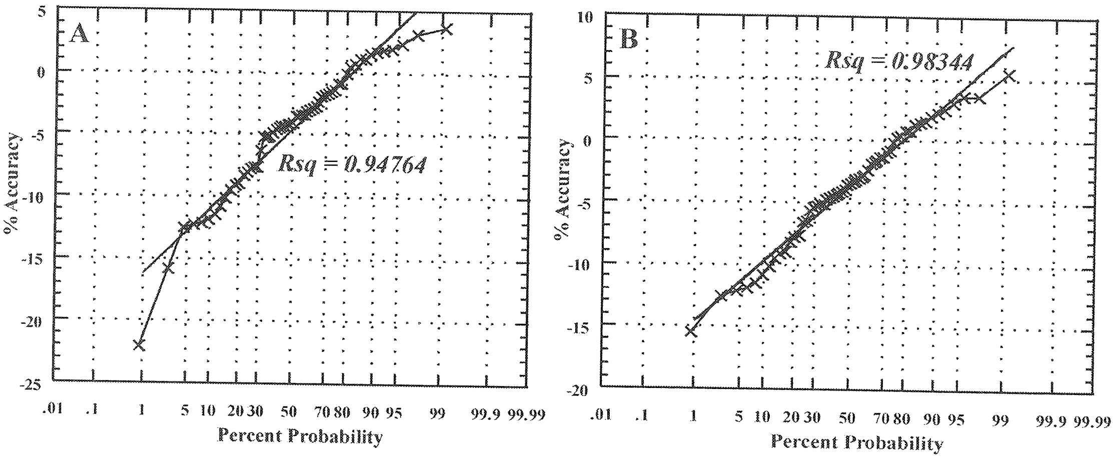

Figure 6.3: Normal probability plots for distribution of DMZC model formation temperature prediction accuracy relative to (**A**) SLEX static temperatures and (**B**) FTEX static temperatures. Crosses represent location of individual data points. *Rsq* refers to the fit of the linear regression.

Histograms of the statistically significant regression static temperature prediction accuracy are presented in Figure 6.4. Standard descriptive statistics for these distributions are as provided in Table 6.2. As for the Horner plot predictions, it appears that the subset of statistically significant regressions is producing, on average, a more accurate estimation of T_{eq} than the population as a whole. Comparison with the average prediction accuracies of the twenty-seven wells which fail the regression F-test appears to confirm this observation (Table 6.3).

Once again, comparison of the significant and non-significant regression result populations may only be undertaken for FTEX data, the non-normal distribution of the SLEX implying application of F or t-tests to this data would be invalid. Application of an F-test for two sample variance at $\alpha = 0.05$ revealed that the population of prediction accuracy from the statistically significant FTEX regression subset should be considered appreciably different to that of the non-significant. This was a slightly different result from the Horner model although once again the F-statistic was close to the critical value (Table 6.4). The apparent difference in

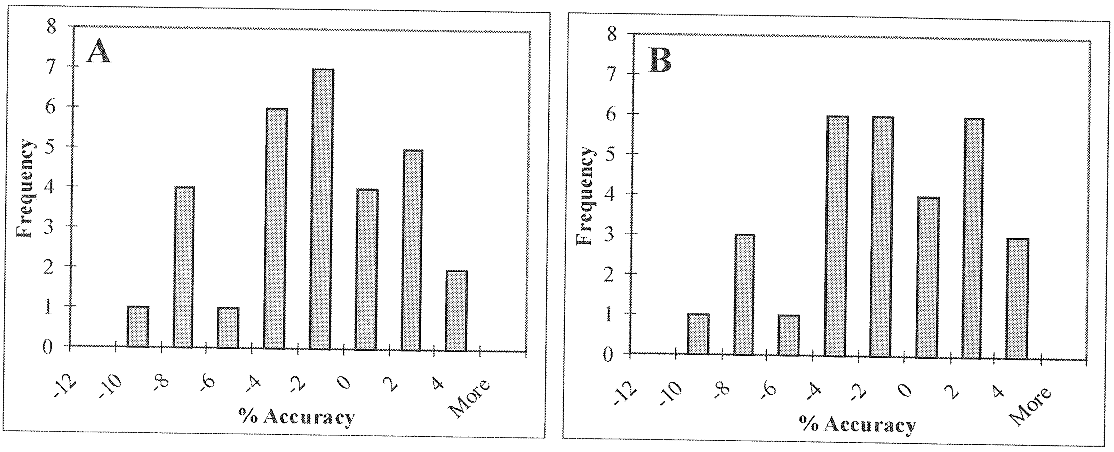

Figure 6.4: Results of DMZC model formation temperature prediction from thirty (30) CBST wells for which the model linear regression passes the F-test for statistical significance. Accuracy is calculated relative to the known static formation temperature, positive numbers indicate percentage over-prediction, negative percentage under-prediction. In graph (**A**) static temperatures are all straight line extrapolated (SLEX), in (**B**) formation compensated static temperatures (FTEX) are used where available.

population variance did not carry through to the two tailed t-test at $\alpha = 0.05$ however, which indicated that, as for the Horner solution, there was no basis for rejecting the null hypothesis. Indeed, there is a probability of 18%, or nearly 1 in 5 chance, that the observed difference between the two population means could be due to chance alone.

	SLEX	**FTEX**
Mean	-3.2	-2.9
Standard Error	0.7	0.7
Median	-3.2	-2.9
Standard Deviation	3.8	3.9
Sample Variance	14.5	14.9
Kurtosis	-0.4	-0.3
Skewness	-0.3	-0.5
Range	15.0	15.0
Minimum	-11.9	-11.9
Maximum	3.1	3.1
Count	30.0	30.0
Confidence Level (95.0%)	1.4	1.4

Table 6.2: Standard descriptive statistics for the histogram distributions of statistically significant DMZC model regression results as given in Figure 6.4.

That the two FTEX populations cannot be distinguished at 95% confidence implies that, as for the Horner model, there may be some factor other than curve fit which is influencing the success of model prediction. Any apparent similarity between the statistics of the Horner and C&J model solutions ended however when the uncertainty in temperature prediction was examined. Calculated average uncertainty (95% confidence) for the statistically significant regressions was found to be ±110%, whilst that for those non-significant regressions was a staggering ±516%. These large uncertainties appear to arise from a combination of two separate effects. Compared to the Horner regressions the range of calculated x-values [1-F(α,τ)] in any given C&J regression was relatively small, implying a high standard error for regression coefficients and consequently broad confidence intervals. Adding to this problem was the fact that, for the C&J model static temperature is determined as the sum of the regression co-efficients *m* (gradient) and *c* (intercept). Calculation of T_{eq} thus effectively compounded the already large error in both variables, significantly increasing the size of the uncertainty.

	SLEX	**FTEX**
Mean	-6.0	-4.6
Standard Error	1.2	1.0
Median	-4.5	-4.2
Standard Deviation	6.0	5.4
Sample Variance	36.2	29.6
Kurtosis	0.4	-0.6
Skewness	-0.7	-0.1
Range	25.7	21.0
Minimum	-22.0	-15.5
Maximum	3.6	5.5
Count	27.0	27.0
Confidence Level (95.0%)	2.4	2.2

Table 6.3: Standard descriptive statistics for the statistically non-significant subset of DMZC model regression results.

Temperature Populations	FTEX
F	1.98
P(F<=f) one-tail	0.04
F Critical one-tail	1.88
t Stat	-1.35
P(T<=t) two-tail	0.18
t Critical two-tail	2.01

Table 6.4: F and t-test results for two sample analysis of statistically significant and non-significant populations of DMZC model prediction accuracy relative to FTEX static temperatures.

6.6 Systematic Uncertainty

Each of the eight parameters necessary for the prediction of T_{eq} using the DMZC source BHT model of C&J is associated with a level of uncertainty. Those parameters which are measured directly carry resolution error as well as the possibility of bias through instrumental or human error. Likewise, those parameters which were estimated are subject to uncertainties inherent in the assumptions required for their prediction. The impact of the uncertainty in each individual parameter upon the overall success of the model depends upon both the magnitude of the error and the sensitivity of the model to the value in question. As demonstrated by t_C in the Horner model, large uncertainty in a single input parameter does not necessarily equate to especially poor prediction quality. In order to evaluate the potential impact of individual parameter uncertainty on the quality of temperatures predicted by the model it was necessary to undertake a systematic analysis of uncertainty.

Seven input parameters are required for the solution of $F(\alpha, \tau)$ and in all cases enter the equation as components of one or both of the ratios α and τ. In order to determine the range of systematic uncertainty in the x-direction it was thus first necessary to determine how these two ratios interacted to maximise or minimise the function. Average values of calculated maximum and minimum α and the first three τ (corresponding to the first, second and third t_L respectively) for the 57 modelled wells are provided in Table 6.5 along with the average of 'optimum' values used in the calculation of T_{eq} above. It is clear from Table 6.5 that, in spite of an apparent increase in magnitude with t_L, the range of uncertainty in τ never exceeds ±40% of the optimum whilst that of α does not go beyond ±20%.

Ratio	Average Minimum	Average Optimum	Average Maximum
α	0.947 (15.66)	1.123	1.327 (18.15)
τ_1	2.121 (39.58)	3.510	4.618 (31.56)
τ_2	4.107 (39.04)	6.737	8.784 (30.39)
τ_3	6.658 (38.66)	10.854	14.069 (29.63)

Table 6.5: The calculated average range of uncertainty in the ratios α, τ_1, τ_2, and τ_3 from 57 CBST wells. Subscripts on τ indicate first, second and third t_L respectively. Optimum values represent those chosen for the estimation of predicted T_{eq}. Values in brackets represent the percentage error *i.e.* the percentage variation from the optimum.

As the complex nature of $F(\alpha, \tau)$ defies attempts to generate an error term by partial differentiation, uncertainty in the function was instead estimated by using a range technique (Appendix 4). In order to assess how the function might respond to the possible range of uncertainty in the ratios α and τ_n a number of different (α, τ_n) pairs were tested and their results compared to that of the optimum solution (Table 6.6). As the two ratios share several input parameters there were limits to the valid (α, τ) combinations which may be entered into the function. It was not correct, for instance, to pair maximum possible α with maximum possible τ as this implied the use of two separate values for ρ_f and c_f. It is for this reason that Table 6.6 contains 'maximised' and 'minimised' intermediate ratio values used in combination with true maximum and minimum possible α and τ.

(α, τ) Combination	Average $F(\alpha, \tau_1)$	Average $F(\alpha, \tau_2)$	Average $F(\alpha, \tau_3)$
(α max, τ min)	0.1626	0.0960	0.0645
(α max, τ ix)	0.1317	0.0770	0.0515
(α min, τ max)	0.1308	0.0743	0.0488
(α min, τ in)	0.1631	0.0937	0.0617
(α in, τ min)	0.1783	0.1062	0.0715
(α ix, τ max)	0.1184	0.0670	0.0439

Table 6.6: The possible range of uncertainty in $F(\alpha, \tau)$ based on the known uncertainty range of input ratios α and τ. Values of $F(\alpha, \tau)$ provided are the average of 57 CBST wells. Subscript 'max' implies the maximum possible value of a ratio (refer Table 6.5), 'min' the minimum possible value. Subscripts 'ix' and 'in' refer to maximised and minimised intermediate values respectively.

Surprisingly, it was found that in all cases combinations of the most extreme ratio values (*e.g.* α_{max} and τ_{min}) did not result in the most extreme value of F(α, τ). Instead, the function appeared to be maximised when minimum possible values of τ were combined with a minimised intermediate value of α and vice versa. This conclusion was supported by plots of F(α, τ) versus α and τ across the ranges $0.5 \leq \alpha \leq 8$ and $0.2 \leq \tau \leq 20$ (Figure 6.5). It is apparent from this figure that, across the positive range of α and τ, F(α, τ) is maximised at minimum possible (α, τ) and minimised at maximum possible (α, τ). In the case of the CBST well data the larger proportionate uncertainty in τ implies that the most extreme values of F(α, τ) occurred when this ratio was set at its limits.

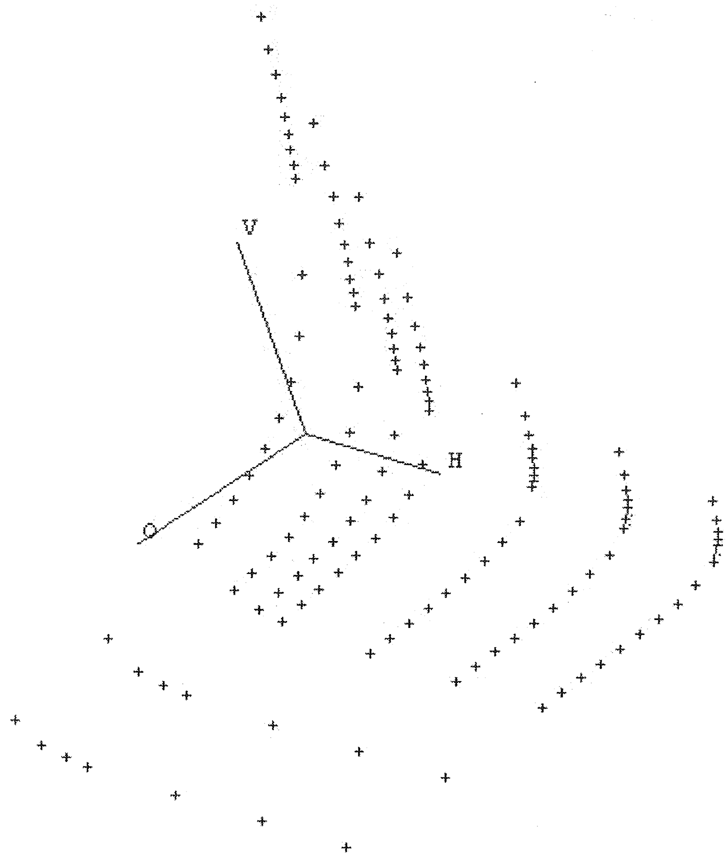

Figure 6.5: Distribution of the function F(α,τ) over the range $0.5 \leq \alpha \leq 8$ and $0.2 \leq \tau \leq 20$. O = τ, H = α, V = F(α,τ).

Using the appropriate combinations of α and τ in F(α, τ) it was possible to calculate values for the systematic uncertainty in the x-direction. As was the case for the Horner model, total error in the x-component F(α, τ) was found to contain both dependent and independent components. An example of a typical calculated error envelope is provided for the well Taloola 2 in Figure 6.6. In this image the total dependent uncertainty in F(α, τ) is represented by maximum and minimum possible regression lines. As for the Horner plot the dependent x-direction uncertainty in the C&J model, which arises out of the combined uncertainty in the constants a, ρ_m, c_m, ρ_f, c_f, and k_f is relatively large. Once again however, conditions of modelling imply that these components cannot vary from point to point, restricting the allowable range of regression lines. Also visible in this figure are error bars which provide an indication of the independent uncertainty present in each point. Aligned in both the x and y directions, the y-error bar represents the estimated resolution limit of the thermometer used to measure a given BHT while the x-error bar is that portion of the horizontal uncertainty in [1-F(α, τ)] which may be attributed to the potential variation in t_L (Appendix 4).

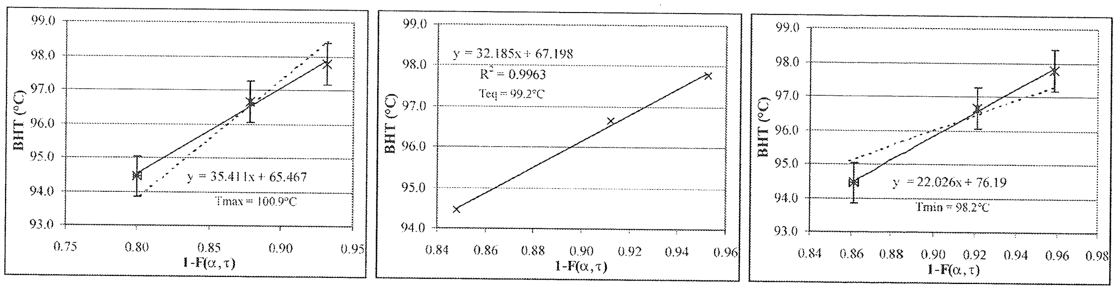

Figure 6.6: Error envelope determined for a typical three-point DMZC model regression in well Taloola 2. The central graph represents the best-fit solution as shown in Figure 6.1. To the left is the upper limit of uncertainty, to the right the lower limit of uncertainty. The solid regression lines in the LHS and RHS graphs represents the limits of regression due to uncertainty in dependent parameters (constants) only. Error bars superimposed upon these limits indicate the uncertainty on these lines due to the independent error in the resolution limits of t_L and BHT. The dotted regression lines indicate the maximum (left) and minimum (right) predictions of T_{eq} possible from the total error envelope (dependent + independent error). Equations for these lines are as shown along with the calculated T_{eq}. Please note the error envelope has been depicted in this way so as to enable the relatively small x-error bars to be visible.

Solving for only that variation produced by error in the constant terms (a, ρ_m, c_m, ρ_f, c_f, k_f) gives the total dependent error which in this case averaged only +0.73; -0.27%

(+0.90; -0.34°C) of predicted T_{eq} for the 57 modelled wells. Total systematic uncertainty in C&J model prediction was then determined graphically for the 48 three point wells by including the effects of independent error in t_L and BHT (Figure 6.6). Results from these wells indicated that, as for the Horner model, the relatively small independent error was again responsible for producing the greatest share of uncertainty in prediction. Total calculated uncertainty in the 48 three-point wells averaged +2.1; -1.5% (+2.6; -1.8°C). Combining these values with those determined for the SLEX temperatures (Chapter 4; Appendix 4) gave an uncertainty in percentage accuracy of –2.6; +1.9%. For the SLEX temperatures this implied a mean overall prediction accuracy range of between –2.0 and –6.5%, confirming the bias in the model. For FTEX temperatures the equivalent range of uncertainty is likely to be larger although this is difficult to quantify.

6.7 Sensitivity Analysis

A number of checks were undertaken in order to determine if the bias recorded within the DMZC C&J model results could be attributed to systematic changes in well characteristics or model input parameters. Box plots of prediction accuracy split along the factors identified in Chapter 4 as having the potential to influence model results are provided in Figure 6.7 along with those for results derived from statistically significant and non-significant regressions. A breakdown of statistically significant wells versus curve type and the number of data points is given in Figure 6.8. Also provided, in Figure 6.9, are a series of scatter plots representing prediction accuracy versus individual input parameters, input ratios α and τ, model fit R^2, CBL extrapolation distance, CBL lag time and t_C.

For both SLEX and FTEX formation temperatures the patterns of population distribution visible in the box plots of Figure 6.7 are almost identical to that of the equivalent Horner model results (Figure 5.6). Once again there appears to be some improvement in average prediction accuracy in those wells characterised by category (2) CBL, type 1 curves, 4 or more data points and statistically significant regressions. Although the subset predictions from statistically significant regression still can not be distinguished from the statistically non-significant at α = 0.05 the greater variance noted between the two is evident as one of the main differences between the C&J and

Horner model results. From Figure 6.8 is it clear that curve shape is again exercising a great influence on the success of regression, whilst the scatter plot of R^2 versus prediction accuracy (Figure 6.9) again implies that any relation between curve fit and the success of temperature prediction is weak at best.

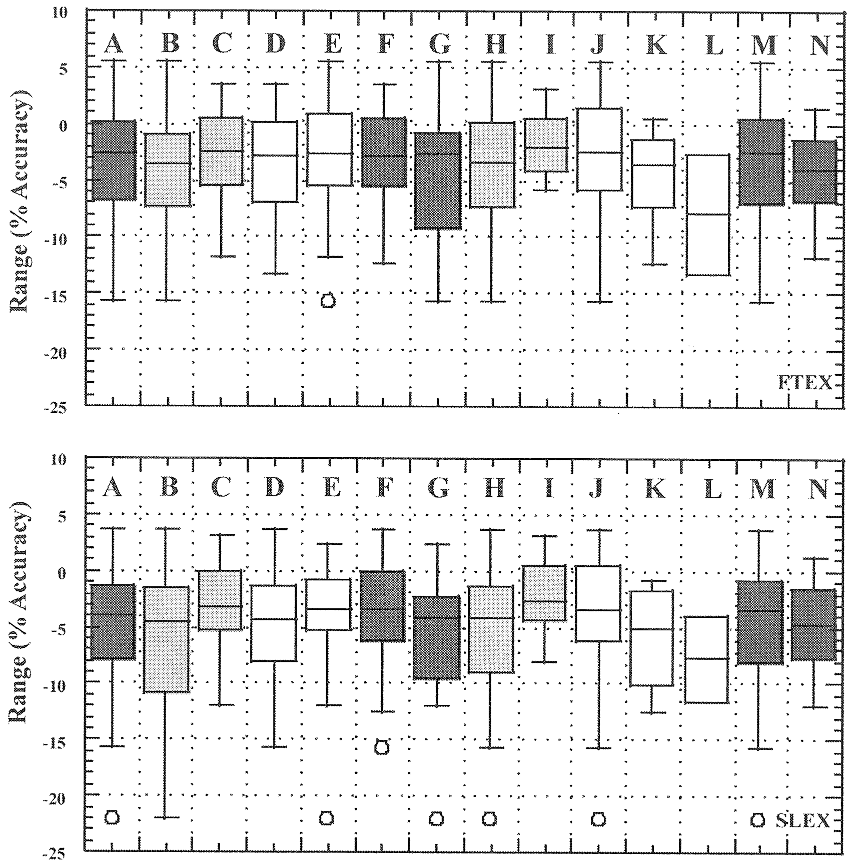

Figure 6.7: Box plots showing population distribution of results of DMZC model formation temperature prediction accuracy relative to FTEX (top) and SLEX (bottom) static temperatures. (**A**) total population (n = 57); (**B**) subset of wells with statistically non-significant regressions (failure of regression F-test; n = 27); (**C**) subset of wells with statistically significant regressions (n = 30); (**D**) subset of wells with CBL category 1 (n = 46); (**E**) subset of wells with CBL category 2 (n = 11); (**F**) subset of wells with no coal bearing formations between CBL and BHT depth (n = 38); (**G**) subset of wells with coal bearing formations between CBL and BHT depth (n = 19); (**H**) subset of wells with three BHT data points only (n = 48); (**I**) subset of wells with four or more BHT data points (n = 9); (**J**) subset of wells with type 1 curves (n = 43); (**K**) subset of wells with type 2 curves (n = 12); (**L**) subset of wells with type 3 curves (n = 2); (**M**) subset of wells with only one recorded pre-logging conditioning episode (n = 49); (**N**) subset of wells with two or more recorded pre-logging conditioning episodes (n = 8).

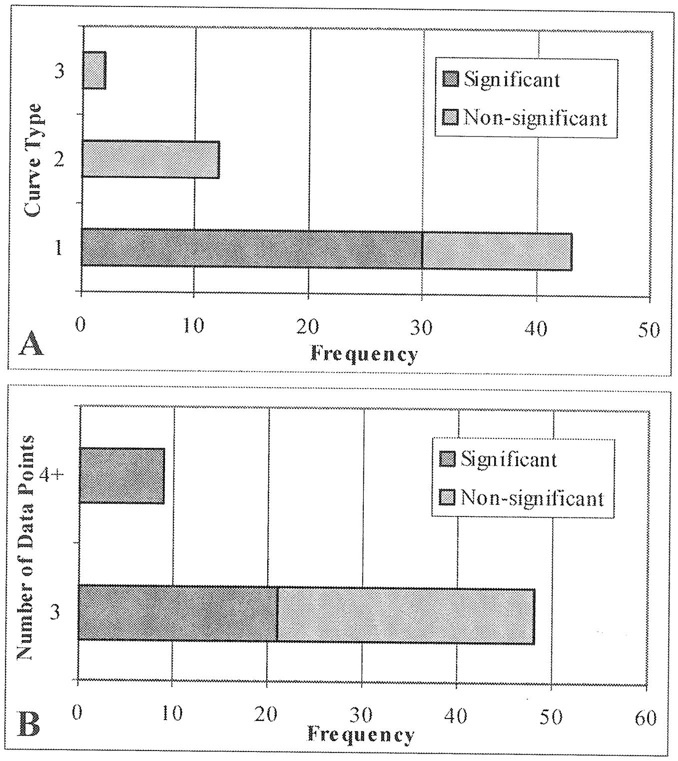

Figure 6.8: Bar graphs illustrating the relationship between the statistical significance of DMZC model regression and (A) curve type; (B) number of available data points.

Of the seven input parameters in α and τ only lag time, t_L and formation density ρ_f appear to show any correlation with the success of model prediction. Once again, the C&J model mirrors the results generated by the Horner solution. With one main exception (Woolkina 2), all wells with initial t_L >7 hours and/or total t_L >20 hours and/or lag window >15 hours are characterised by prediction accuracies close to ±5% of the FTEX static temperature. As for the Horner predictions SLEX results are virtually equivalent to FTEX with the sole addition of a second outlier, the well Ulandi 2. The influence of lag time on prediction accuracy is further reflected in this model by the ratio τ which shows a positive correlation to %Accuracy. In this sense τ is notably different to α which does not appear to bear a systematic control on prediction. It is clear from Figure 6.9 that prediction accuracies for wells with initial τ >5 and/or final τ >15 and/or a total τ interval >10 appear to be unbiased and very close to within ±5% of both estimates of static temperature. The apparent influence of ρ_f may be explained in light of this fact as it, along with t_L, enters into the ratio τ. As t_L appears in the numerator and ρ_f in the denominator of the ratio it is logical that increasing t_L be associated with improved prediction whilst increasing formation

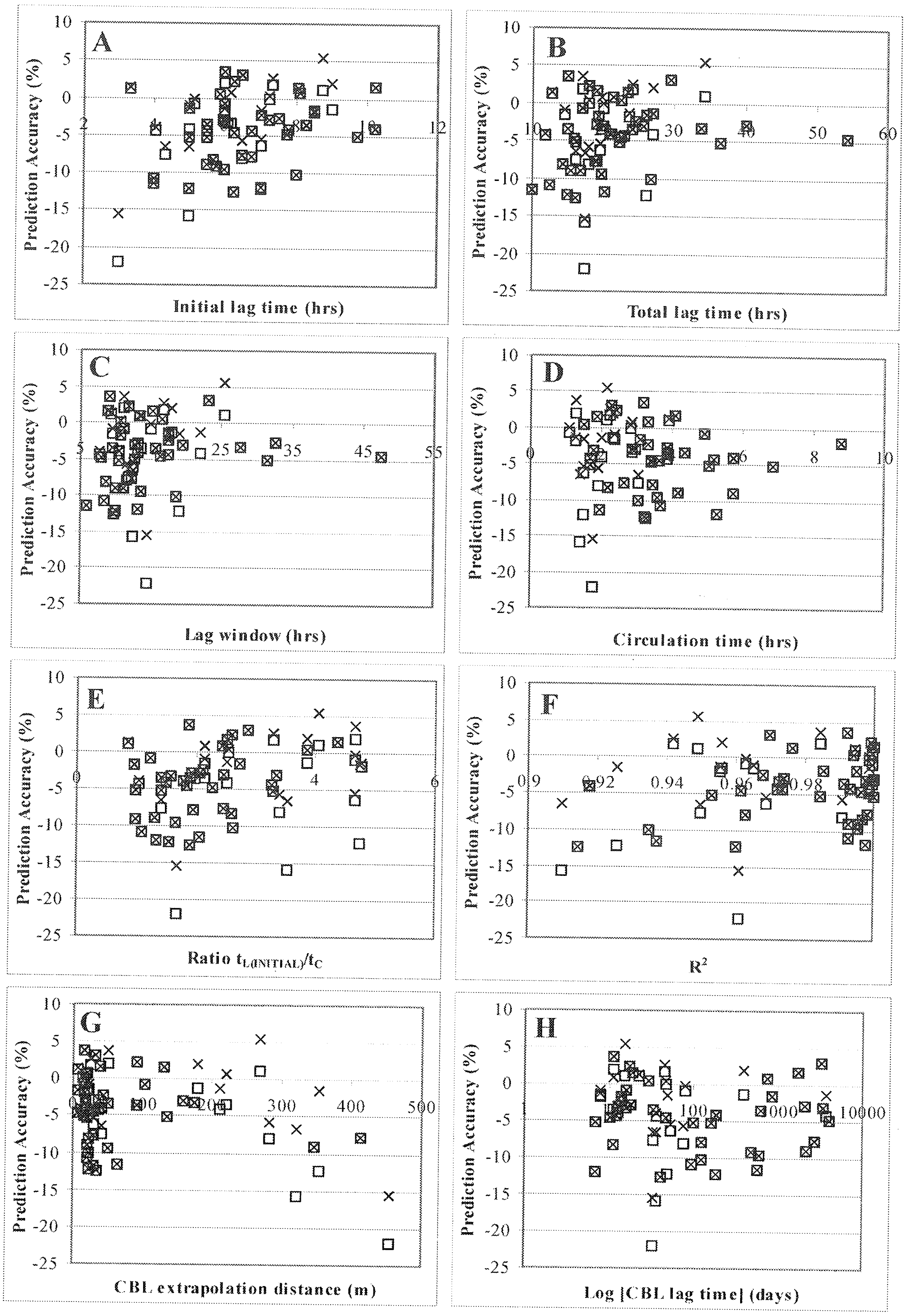

Figure 6.9: Scatter graphs depicting the accuracy of DMZC model formation temperature prediction as percentage difference from estimated SLEX (squares) and FTEX (crosses) static temperature for 57 CBST wells versus (**A**) initial BHT lag time; (**B**) final BHT lag time (total lag time); (**C**) lag window (final – initial lag times); (**D**) total circulation time; (**E**) the ratio of initial lag time to total circulation time; (**F**) model fit (R^2); (**G**) the extrapolation distance of the CBL temperature; (**H**) the CBL lag time; (**I**) heat capacity of the mud; (**J**) heat capacity of the formation; (**K**) mud density; (**L**) formation density; (**M**) formation thermal conductivity; (**N**) initial tau value; (**O**) final tau value (total tau); (**P**) tau window (final – initial tau) and (**Q**) alpha constant.

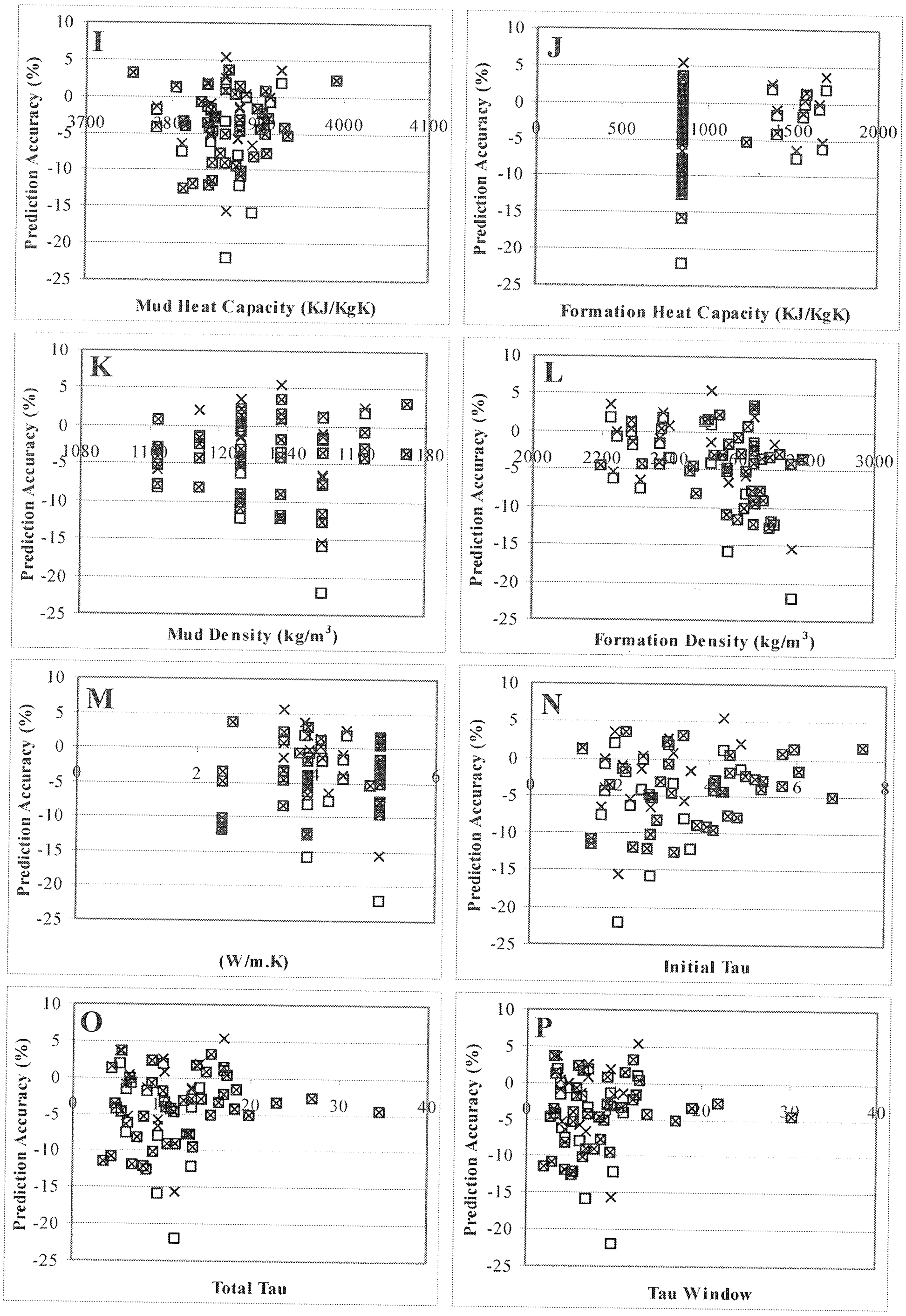

Figure 6.9: Scatter graphs depicting the accuracy of DMZC model formation temperature prediction as percentage difference from estimated SLEX (squares) and FTEX (crosses) static temperature for 57 CBST wells versus (**A**) initial BHT lag time; (**B**) final BHT lag time (total lag time); (**C**) lag window (final – initial lag times); (**D**) total circulation time; (**E**) the ratio of initial lag time to total circulation time; (**F**) model fit (R^2); (**G**) the extrapolation distance of the CBL temperature; (**H**) the CBL lag time; (**I**) heat capacity of the mud; (**J**) heat capacity of the formation; (**K**) mud density; (**L**) formation density; (**M**) formation thermal conductivity; (**N**) initial tau value; (**O**) final tau value (total tau); (**P**) tau window (final – initial tau) and (**Q**) alpha constant.

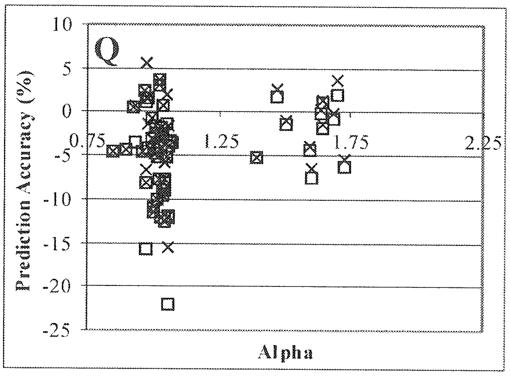

Figure 6.9: Scatter graphs depicting the accuracy of DMZC model formation temperature prediction as percentage difference from estimated SLEX (squares) and FTEX (crosses) static temperature for 57 CBST wells versus (**A**) initial BHT lag time; (**B**) final BHT lag time (total lag time); (**C**) lag window (final – initial lag times); (**D**) total circulation time; (**E**) the ratio of initial lag time to total circulation time; (**F**) model fit (R^2); (**G**) the extrapolation distance of the CBL temperature; (**H**) the CBL lag time; (**I**) heat capacity of the mud; (**J**) heat capacity of the formation; (**K**) mud density; (**L**) formation density; (**M**) formation thermal conductivity; (**N**) initial tau value; (**O**) final tau value (total tau); (**P**) tau window (final – initial tau) and (**Q**) alpha constant.

density results in a deterioration. Of the other parameters which enter τ, well radius and formation heat capacity are constant for most wells. The exception to the latter case are wells which terminate in known aquifer sequences. Here, a relative increase in c_f is offset by an associated decrease in ρ_f and prediction accuracy does not appear to be affected. Surprisingly, formation thermal conductivity k_f does not appear to correlate well with accuracy despite its presence in the numerator of τ, a fact probably accounted for by its relatively small magnitude.

It is clear from these results that formation temperature prediction from the C&J DMZC model is, to all intents, very similar to that of the Horner model. Once again the lag time of the available data appears to be the main controlling influence on the accuracy of the predicted T_{eq}. This implies that the C&J model must be functioning in a similar way to that of the Horner plot and is probably breaking down at short lag times. As a consequence, those wells characterised by longer total lag time and/or windows of lag time are once again producing the most accurate temperature predictions. The implication arising from these results will be discussed further in Chapter 9.

CHAPTER 7

TESTING THE SEMI-LOG PLOT

7.1 Introduction

Mathematically, the semi-log plot is based upon an empirical assumption that BHT recovery is related directly, and only, to elapsed lag time. It is the most straightforward of all the BHT recovery models, requiring no knowledge of circulation time or of the thermal properties of the formation or well contents. The form of the semi-log plot is close enough to that of the Horner model that it seems likely it was devised specifically as a sort of 'zero-circulation' Horner plot. There is no mathematical justification for this derivation however as the line source model (LSM) upon which the Horner plot is based implicitly requires circulation time. The absence of circulation time in the LSM would in fact imply that there was no thermal disturbance and thus no need to model a temperature correction.

Nevertheless, in spite of these inconsistencies, the empirical semi-log method continues to be used for the determination of true formation temperature. Perhaps because of its simplicity, and because circulation time is often poorly constrained, it has become the model of choice for industry within the Cooper Basin and examples of its application are found in most WCR. That the semi-log plot is considered a reasonable substitute for the Horner model is illustrated by Pitt (1986) who claims that semi-log and Horner models, when applied to the same data, produce estimates of T_{eq} which 'commonly match to within two percent'.

7.2 The Problem of Extrapolation

Outwardly similar to a Horner plot, the semi-log plot differs from the LSM in a number of important ways. Perhaps the most significant discrepancy between the two techniques is the extrapolation of the linear regression to find T_{eq}. In a Horner plot infinite lag time corresponds to the y-intercept and T_{eq} is estimated by extrapolation to $x = 0$. In a semi-log plot, however, lag time itself lies along the x-axis implying T_{eq} is determined by extrapolation to some arbitrarily large value of time. The great dilemma of the semi-log plot is thus what length of time is sufficient for full thermal equilibration. If the chosen interval is too small we may expect an under-prediction of T_{eq}. If it is too large then the result will be an over-prediction, the linear nature of the plot implying predicted T_{eq} will simply increase indefinitely as $t_L \rightarrow \infty$.

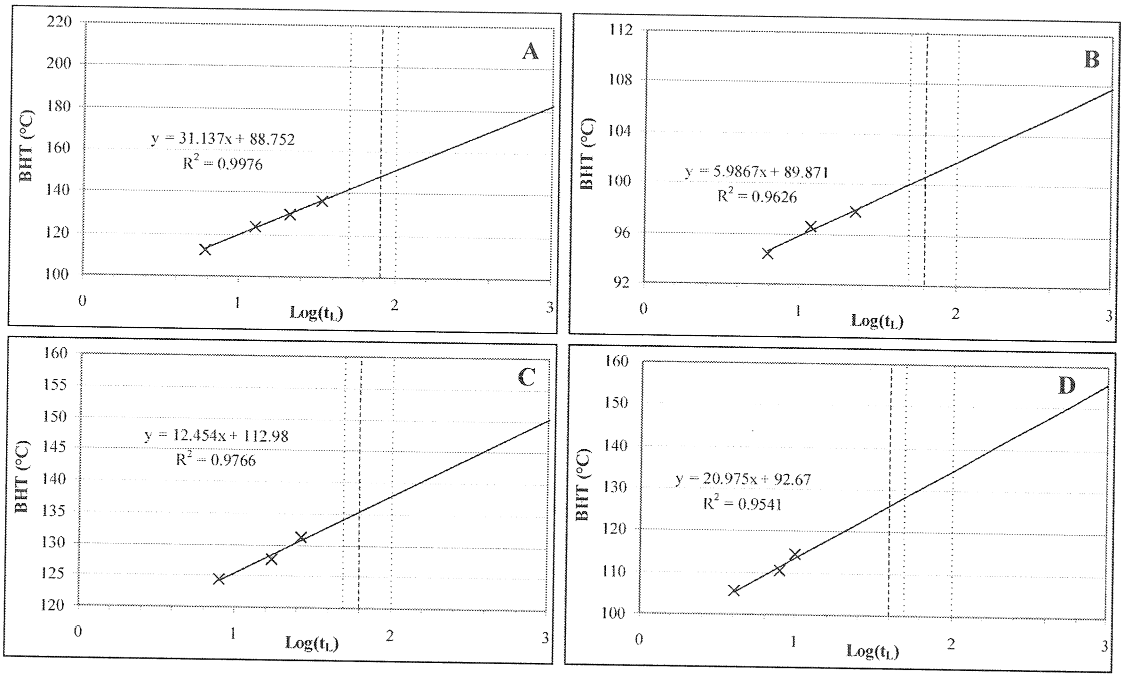

Figure 7.1: Typical examples of semi-log plot model regression. Predicted equilibrium temperature is given by the value of y calculated after extrapolation of the regression line to a given time. Dotted vertical lines indicate extrapolations to 50 hours (x = 1.7) and 100 hours (x = 2). The dashed vertical line indicates extrapolation to twenty times the known circulation time. (A) Bookabourdie 2 (SLEX = 144.3); (B) Taloola 2 (SLEX = 104.2); (C) Woolkina 2 (SLEX = 148.8) and (D) Della 10 (SLEX = 138.1). Refer to Figure 4.6 for comparison with the primary temperature-time data curves.

Pitt (1986) suggested appropriate extrapolation times for semi-log plots were of the order of 10 to 100 days. Bullard (1947) however concludes that the bottom-hole region of a recently drilled well should recover to within 1% of its original temperature within a period of 10-20 times the duration of the EOH circulation. For most CBST wells this would imply that extrapolation time should, on average, be between 30 and 60 hours. Bullard's argument appears to be supported by the results of semi-log plot static temperature estimation within the WCR which are derived from extrapolation times of between 30 and 50 hours. Although these values are routinely lower than CBL temperatures, they are not so much lower as to suggest the need for several days more equilibration. It seems likely then, that the extrapolation time required for accurate estimation of true formation temperature is of the order of hours rather than days and may be close to 20 times the length of t_C. It is important to note however, that using an extrapolation time based upon t_C means this parameter must be known. This is something of a contradictory situation given that the semi-log model appears to have been designed specifically for use in wells where this data is not available.

7.3 Application of the Semi-log Plot

Application of the Semi-log plot generates a single regression line, the equation for which may then be used to estimate various values of T_{eq} by extrapolation to different lag times (x). Examples of graphical results produced by application of the Semi-log model to selected CBST wells are presented in Figure 7.1. As values of estimated circulation time do exist for all graded wells it was decided to test the purported independence of the semi-log model to this parameter. This was undertaken by comparing model results generated by using extrapolation time equal to 20 times the circulation with those generated by using arbitrary times of 50, 100 and 1000 hours.

7.4 Model Results

Overall, the fit of the semi-log regressions to the available data was good with average calculated R^2 equal to 0.9651 for all sixty-one modelled wells. Only four wells stood out with values of $R^2 < 0.9$. This group comprises the type 3 curve Spencer 5, the fast recovery curve of Burke 1 and similarly shaped Biala 1 as well as the four-point data curve of Dullingari 40. The latter case represents the first and only time a four data-point well has failed to display a model fit greater than $R^2 = 0.9$, although at $R^2 = 0.889$ it is only slightly below the cut. Statistical analysis of this regression using the F-test indicated that, despite the reduced model fit, it should be considered significant at $\alpha = 0.05$. For this reason it was decided to retain this well for further consideration although the other three poor model fits were excluded. Adjusted average R^2 for the remaining 58 wells is 0.979.

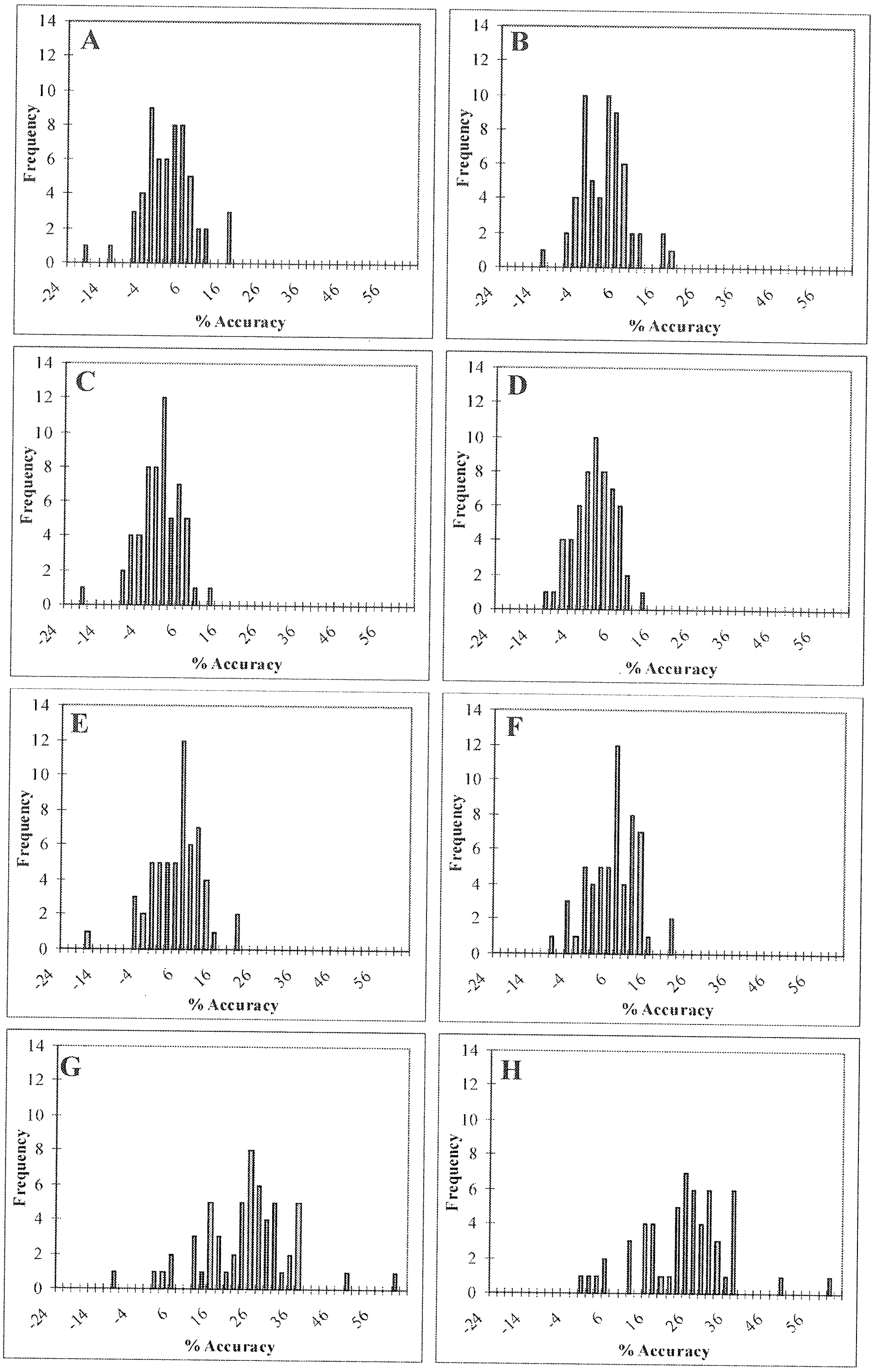

Figure 7.2: Results of semi-log plot formation temperature prediction for fifty-eight (58) CBST wells. Accuracy is calculated relative to the known static formation temperature, positive numbers indicate percentage over-prediction, negative percentage under-prediction. Graphs (**A**) and (**B**) results are from extrapolation to 20 times the known circulation time relative to SLEX and FTEX static temperatures respectively; (**C**) and (**D**) extrapolation to 50 hours relative to SLEX and FTEX static temperatures respectively; (**E**) and (**F**) extrapolation to 100 hours relative to SLEX and FTEX static temperatures respectively and (**G**) and (**H**) extrapolation to 1000 hours relative to SLEX and FTEX static temperatures respectively.

Histograms comparing the results of semi-log plot static temperature prediction for values of extrapolation time equal to 20 times the total estimated circulation time ($20*t_C$), 50, 100 and 1000 hours to SLEX and FTEX static temperatures respectively are presented in Figure 7.2. A complete set of standard descriptive statistics for these results is included in Table 7.1. It is clear from these results that, as expected, T_{eq} becomes progressively more over-predicted as extrapolation time increases. Extrapolation to 1000 hours results in average over-prediction greater than 20% for both SLEX and FTEX temperatures. This value decreases to around 4% for extrapolation to 100 hours. Clearly, the assertion of Pitt (1986) that extrapolation times of 10 to 100 days are appropriate for the semi-log model is not correct for Cooper Basin data.

Extrapolation Time	**$20*t_C$**		**50hrs**		**100hrs**		**1000hrs**	
Static Temperature	**SLEX**	**FTEX**	**SLEX**	**FTEX**	**SLEX**	**FTEX**	**SLEX**	**FTEX**
Mean	-0.4	0.3	-1.9	-1.2	3.6	4.4	21.9	22.8
Standard Error	0.9	0.8	0.7	0.7	0.9	0.8	1.5	1.5
Median	0.0	0.7	-1.8	-1.2	4.6	5.1	23.5	23.7
Standard Deviation	6.6	6.0	5.3	5.0	6.5	6.2	11.5	11.2
Sample Variance	43.8	36.3	28.0	25.2	42.3	38.6	133.2	126.5
Kurtosis	1.5	0.6	1.4	-0.3	1.4	0.1	1.9	1.4
Skewness	0.0	0.4	-0.5	-0.2	-0.4	-0.2	0.1	0.1
Range	37.0	30.6	30.5	24.0	37.0	30.4	70.3	62.9
Minimum	-21.1	-14.5	-20.1	-13.4	-18.0	-11.1	-11.1	-3.7
Maximum	15.9	16.1	10.4	10.6	19.0	19.2	59.2	59.2
Count	58.0	58.0	58.0	58.0	58.0	58.0	58.0	58.0
Confidence Level (95.0%)	1.7	1.6	1.4	1.3	1.7	1.6	3.0	3.0

Table 7.1: Standard descriptive statistics for the histogram distributions of semi-log plot results given in Figure 7.2. Extrapolation times are as shown.

It is difficult to distinguish the most successful semi-log model, with mean results for the $20*t_C$ and 50 hour extrapolation time appearing to be quite close. While the $20*t_C$ results appear to be more accurate on average, the 50 hour results are more precise. That the two models are similar is perhaps not surprising given that the average numerical value of $20*t_C$ for the fifty-eight modelled wells is around 69.2 hours. In fact, the 50 hour extrapolation is well within error of average $20*t_C$, the large systematic uncertainty in t_C implying a possible range for the latter of 34 to 116 hours. In both cases mean prediction accuracy for the SLEX and FTEX reflect the general trend first noted in the Horner results where FTEX results are more positive than SLEX and are characterised by a reduced range. Although no significant skew is detected in any of the four result sets, the method of Tabachnich & Fidell (1996) indicates that both SLEX distributions are characterised by a small but significant positive kurtosis. Probability plots of all four result sets are given in Figure 7.3. In both cases the presence of kurtosis in the SLEX results does not appear to cause a significant deviation in the pattern of population distribution relative to the FTEX. As a result, all four population distributions are considered to be effectively normal, although for both SLEX and FTEX results the 50 hour model is noticeably more ideal than the 20*t_C.

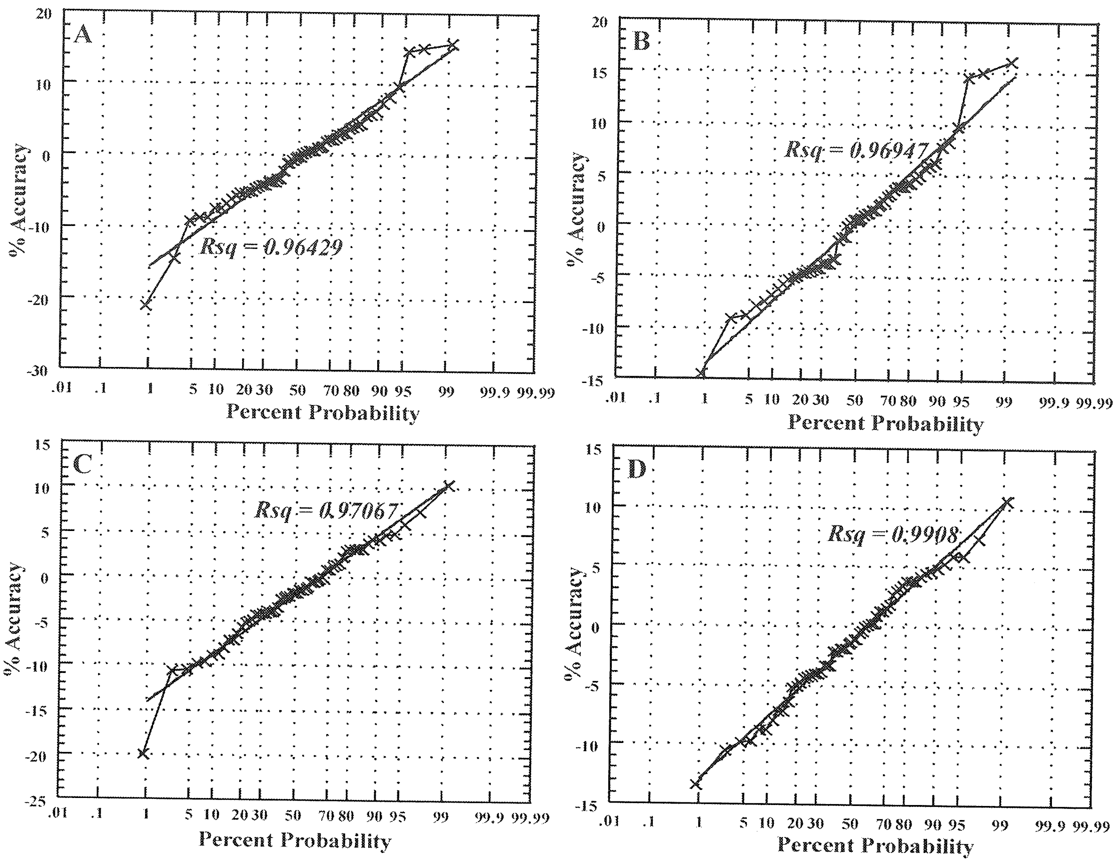

Figure 7.3: Normal probability plots for distribution of semi-log plot formation temperature prediction accuracy. Graphs (**A**) and (**B**) are results from extrapolation to twenty times the known circulation time relative to SLEX and FTEX static temperatures respectively. Graphs (**C**) and (**D**) are results from extrapolation to fifty hours relative to SLEX and FTEX static temperatures respectively. Crosses represent location of individual data points. *Rsq* refers to the fit of the linear regression.

The results generated from the semi-log plot would seem to support the theory of Bullard (1947) by indicating that EOH temperature recovery is likely to occur within a time period around twenty times t_C. For semi-log plots of BHT from the Cooper Basin, where circulation time is relatively small, this implies extrapolation times of between 50 – 100 hours after drilling. This range may be narrowed somewhat by using the known static temperatures to work backward through the semi-log model and thus determine an 'ideal' average extrapolation time. Upon doing so it was found that, with four exceptions, individual well SLEX and FTEX static temperatures all required extrapolation times of less than 250 hours. The four excepted wells (Brumby 4, Fly Lake 2, Kobari 1 and Woolkina 2) are characterised by extrapolation times of over 500 hours, in one case (Kobari 1; SLEX) up to 41728 hours! Such lengthy predicted extrapolation times appear to result from a combination of slow temperature recovery rate and large differences between the known static temperature and the last measured BHT. In the case of Brumby 4, slow temperature recovery could be related

	SLEX	FTEX
Mean	2.2	2.2
Standard Error	0.7	0.7
Median	2.4	2.1
Standard Deviation	5.1	4.9
Sample Variance	25.6	24.2
Kurtosis	0.0	-0.3
Skewness	0.3	0.2
Range	23.4	23.1
Minimum	-7.7	-8.2
Maximum	15.7	14.8
Count	54.0	54.0
Confidence Level (95.0%)	1.4	1.3

Table 7.2: Standard descriptive statistics for the histogram distributions of semi-log plot results given in Figure 7.4. Extrapolation time used is equal to the average calculated ideal for both SLEX and FTEX static temperatures.

to extra circulation experienced by this well during trouble time after the end of drilling. In Kobari 1 the extreme extrapolation time required to reach the SLEX temperature is reduced by an order of magnitude (to 3104 hours) by the use of an adjusted FTEX static temperature. No such explanations are available for Fly Lake 2 or Woolkina 2 however. It may be that the behaviour of these wells is related to the size of their respective BHT data windows and/or the portion of the recovery curve they represent. In the latter case, Woolkina 2, it is the third time that this well has been singled out as exceptional, indicating there may be some undetected bias within the dataset. In any event, for the fifty-four remaining wells, average 'ideal' extrapolation time for SLEX and FTEX static temperatures are 76.4 and 70.3 hours respectively.

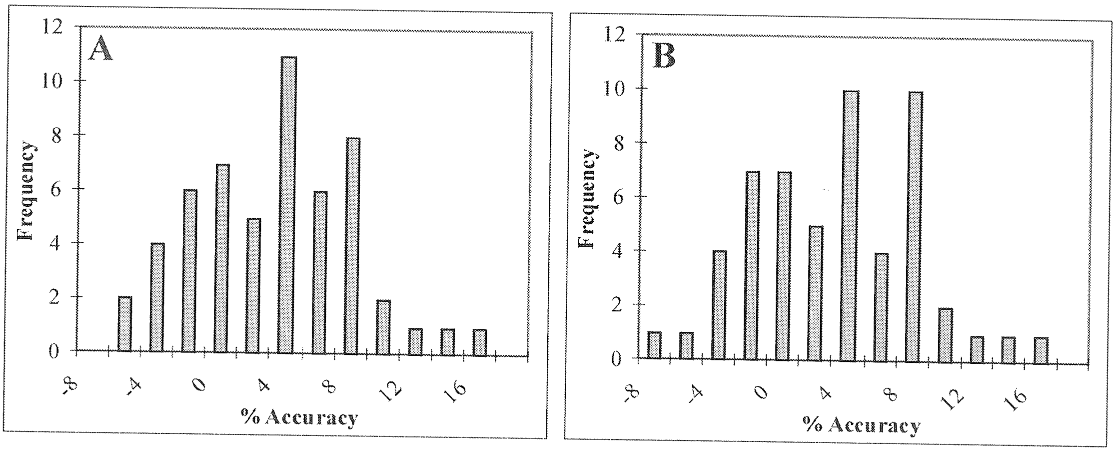

Figure 7.4: Results of semi-log plot formation temperature prediction for fifty-eight (58) CBST wells using average ideal extrapolation time as determined from known static temperatures. Accuracy is calculated relative to the known static formation temperature, positive numbers indicate percentage over-prediction, negative percentage under-prediction. Graph (**A**) results are from extrapolation to calculated ideal extrapolation time based on SLEX static temperatures (t = 76.4 hours). Graph (**B**) results use FTEX static temperatures (t = 70.3 hours) where available.

Substituting the calculated average values for ideal extrapolation time back into forward semi-log models for the same set of 54 wells resulted in prediction distributions that were, once again, biased toward over-estimation (Figure 7.4). Not surprisingly the use of the tailored values produced near-identical results for SLEX and FTEX temperatures with mean predicted over-estimation equal to 2.2% in both cases (Table 7.2). Although use of the 'ideal' average estimation time failed to remove bias from the mean it did result in noticeable reductions in range and standard deviation compared to both the 20*t_C and 50 hours models. An explanation for the persistent bias in these results may lie in the distribution of the calculated 'ideal'

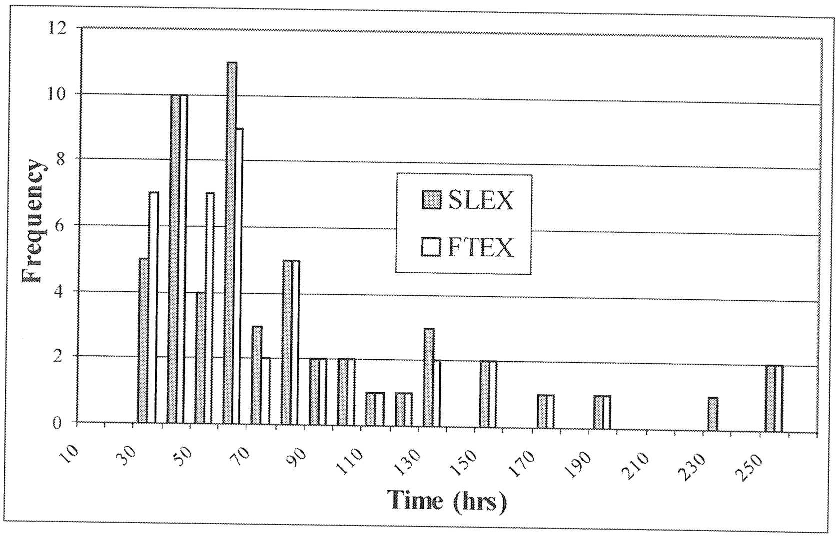

Figure 7.5: Distribution of ideal semi-log plot extrapolation times calculated for fifty-four (54) CBST wells using known static temperatures.

extrapolation times. This population is strongly skewed toward the right, accounting for the bias toward over-prediction when using the 'ideal' average time as well as the slight negative bias observed for the 50hr extrapolation time (Figure 7.5). The range of this data indicates that the semi-log plot should be best solved via the use of individual well-based extrapolation times, such as 20^*t_C. The accuracy of these solutions is limited however, by both the uncertainty in t_C and the need to pick an arbitrary value by which to multiply t_C. Indeed, using the average 'ideal' multipliers of 27.5 (SLEX) and 23.9 (FTEX) (calculated as the average of ideal predicted extrapolation time divided by actual t_C) still results in a bias towards over-prediction and fails to improve substantially on the use of an arbitrary ideal time (Figure 7.6).

7.5 Statistical Analysis

Of the fifty-eight available C&J regressions only twenty-eight pass the regression F-test at $\alpha = 0.05$ and may therefore be considered to be statistically significant. This subset includes all wells with four or more data points and those wells with three data points for which $R^2 > 0.995$. Average R^2 of the significant regressions is 0.989, that of the thirty rejected is 0.9693.

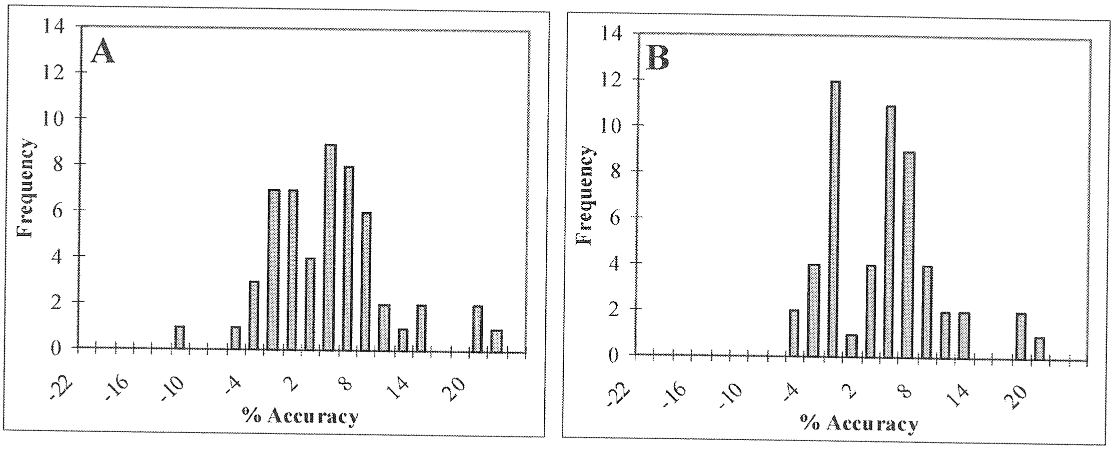

Figure 7.6: Results of semi-log plot formation temperature prediction for fifty-eight (58) CBST wells using average ideal multipliers for known individual circulation times as determined from known static temperatures. Accuracy is calculated relative to the known static formation temperature, positive numbers indicate percentage over-prediction, negative percentage under-prediction. Graph (**A**) results are from extrapolation to calculated ideal extrapolation time based on SLEX static temperatures ($t = 27.5*t_C$). Graph (**B**) results use FTEX static temperatures ($t = 23.9*t_C$) where available.

Histograms of the static temperature prediction accuracy from statistically significant regressions for both $20*t_C$ and 50 hour extrapolations are presented in Figure 7.7. Standard descriptive statistics for these distributions are provided in Table 7.3.

Extrapolation Time	**20*t_C**		**50hrs**	
Static Temperature	**SLEX**	**FTEX**	**SLEX**	**FTEX**
Mean	0.9	1.6	-1.2	-0.5
Standard Error	1.4	1.3	1.1	1.0
Median	0.5	1.5	-0.8	-0.5
Standard Deviation	7.6	6.9	6.0	5.5
Sample Variance	58.0	48.1	36.5	30.5
Kurtosis	1.9	0.5	2.4	-0.1
Skewness	-0.2	0.3	-0.9	-0.2
Range	37.0	30.6	30.5	24.0
Minimum	-21.1	-14.5	-20.1	-13.4
Maximum	15.9	16.1	10.4	10.6
Count	28.0	28.0	28.0	28.0
Confidence Level (95.0%)	3.0	2.7	2.3	2.1

Table 7.3: Standard descriptive statistics for the histogram distributions of statistically significant semi-log plot regression results given in Figure 7.7.

Comparisons of the results in Table 7.3 with those from the whole population (Table 7.1) show no distinct patterns of improvement in prediction accuracy for the statistically significant regressions. In fact, for three out of four cases, wells with statistically significant regressions appear, on average, to be predicting less accurate values of T_{eq}. In all four instances the range of prediction in the high quality regressions is the same as that for the population as a whole resulting in higher standard deviations in the smaller subset. Examination of result quality in the sub-set of thirty statistically non-significant regressions (Table 7.4) also indicates no obvious improvement in accuracy, although in all four of these cases the range of prediction is reduced relative to the population as a whole.

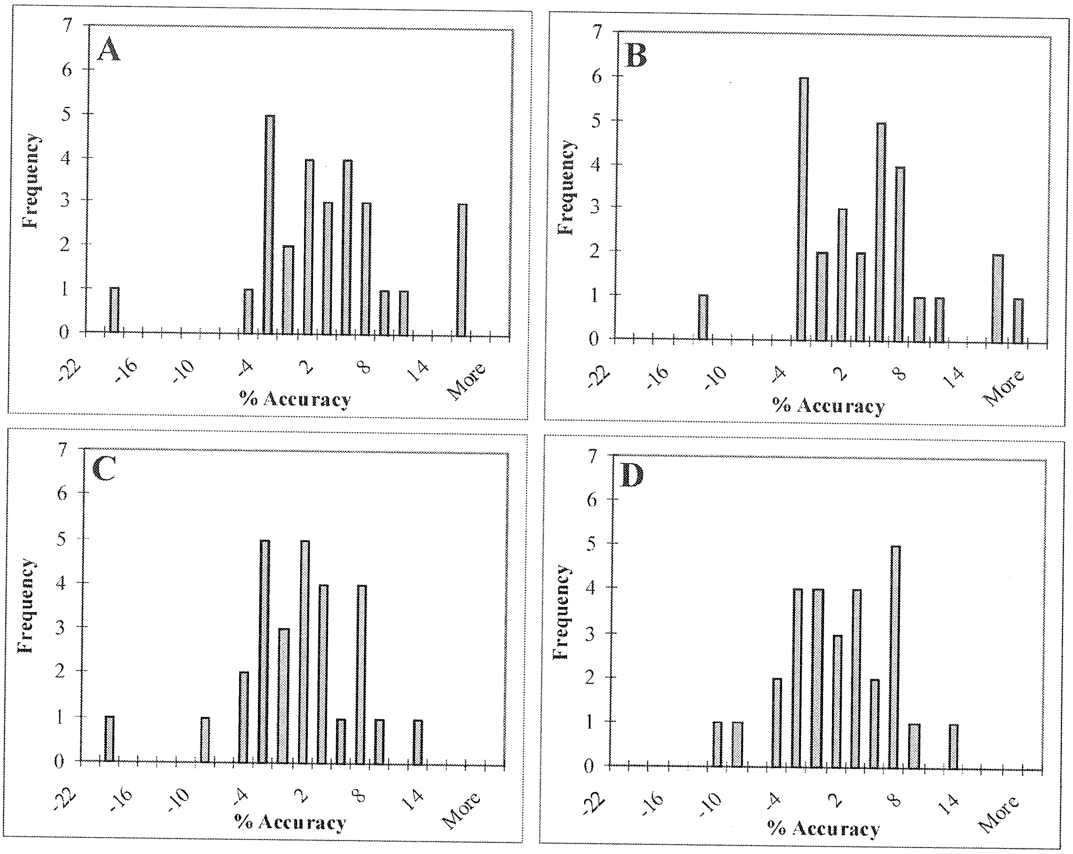

Figure 7.7: Results of semi-log plot formation temperature prediction from twenty-eight (28) CBST wells for which the model linear regression passes the F-test for statistical significance. Accuracy is calculated relative to the known static formation temperature, positive numbers indicate percentage over-prediction, negative percentage under-prediction. Graphs (**A**) and (**B**) are results from extrapolation to twenty times the known circulation time relative to SLEX and FTEX static temperatures respectively. Graphs (**C**) and (**D**) are results from extrapolation to 50 hours relative to SLEX and FTEX static temperatures respectively.

Extrapolation Time	$20*t_C$		50hrs	
Static Temperature	SLEX	FTEX	SLEX	FTEX
Mean	-1.6	-2.6	-0.9	-1.8
Standard Error	1.0	0.8	0.9	0.8
Median	-1.3	-2.0	0.7	-1.4
Standard Deviation	5.4	4.5	4.8	4.5
Sample Variance	28.9	20.2	23.4	20.3
Kurtosis	-0.3	-0.9	-0.9	-0.8
Skewness	-0.2	-0.2	0.0	-0.3
Range	22.8	15.0	17.4	15.8
Minimum	-14.5	-10.7	-9.1	-9.8
Maximum	8.3	4.3	8.3	6.0
Count	30.0	30.0	30.0	30.0
Confidence Level (95.0%)	2.0	1.7	1.8	1.7

Table 7.4: Standard descriptive statistics for the statistically non-significant subset of semi-log plot regression results.

Application of a two-sample F-test for variance to the $20*t_C$ data indicated that at $\alpha = 0.05$, the subset of statistically significant regressions had a meaningful difference in population variance to those of the non-significant (Table 7.5). By contrast the same test applied to the 50 hour models revealed no significant disparity. All cases failed the appropriate two sample t-test however implying the statistically significant and non-significant regression populations cannot be considered appreciably different at 95% confidence (Table 7.5). This, combined with the apparent lack of improvement in result accuracy with regression quality, indicates that the relation between curve fit and model success is weak.

Extrapolation Time	$20*t_C$		50hrs	
Temperature Populations	SLEX	FTEX	SLEX	FTEX
F	2.01	2.06	1.81	1.51
P(F<=f) one-tail	0.03	0.03	0.06	0.14
F Critical one-tail	1.88	1.88	1.88	1.88
t Stat	1.47	1.59	0.96	0.96
P(T<=t) two-tail	0.15	0.12	0.34	0.34
t Critical two-tail	2.01	2.01	2.00	2.00

Table 7.5: F and t-test results for two sample analysis of statistically significant and non-significant populations of semi-log plot prediction accuracy relative to SLEX and FTEX static temperatures.

Unlike previous models, where the statistical uncertainty of temperature prediction was given by the 95% confidence interval of the regression co-efficients, statistical uncertainty of the semi-log plot prediction is given by the 95% prediction limit at the value of t_L to which it is extrapolated. The act of extrapolating the regression line beyond the limit of the data creates a large statistical uncertainty in predicted temperature. For the 50 hour model average prediction limit of the statistically significant wells is ±8.2°C (±6.3%) while for that of $20{*}t_C$ it is ±9.6°C (±7.0%). Equivalent uncertainty on regressions which fail the F-test are noticeably larger averaging ±37.7°C (±29.0%) for the 50 hour model and ±41.7°C (±30.5%) for the $20{*}t_C$.

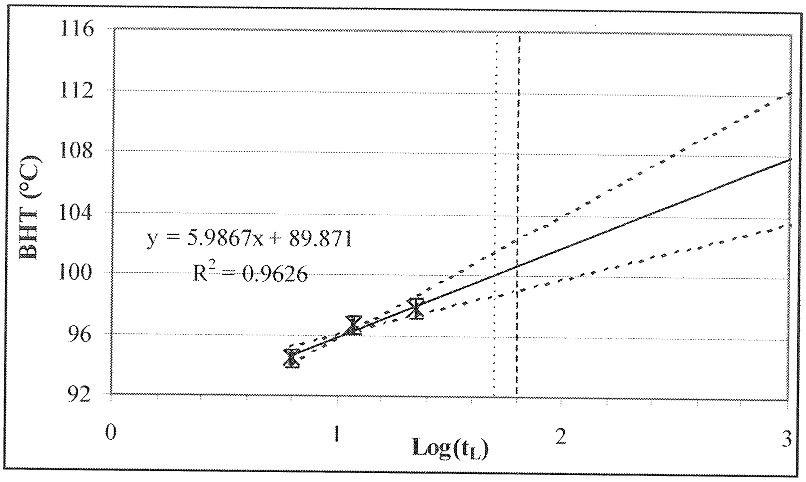

Figure 7.8: Error envelope determined for a typical three-point semi-log plot model regression in well Taloola 2. Independent error in x (t_L) and y (BHT) directions are indicated by error bars. The solid regression line indicates the best fit solution as shown in Figure 7.1. The dotted regression lines indicate the extents of the calculated error envelope. The vertical lines indicate extrapolation times equal to 50 hours (dots) and $20{*}t_C$ (dashes).

7.6 Systematic Uncertainty

Systematic uncertainty in the semi-log plot is derived entirely from resolution error on the primary input parameters t_L and BHT. The magnitude of this uncertainty is illustrated in Figure 7.8 where an error envelope is defined around the regression line by a series of x (t_L) and y (BHT) error bars on each data point. Two things are apparent from this figure, first that the error is entirely independent, second that the error envelope will continuously diverge with increasing extrapolation time.

For the forty-nine three data-point wells the calculation of systematic uncertainty in estimated T_{eq} was relatively trivial, graphical methods indicating average uncertainties of +2.0°C; -1.9°C (+1.6%; -1.5%) for the 50 hour model and +2.4°C; -2.3°C (+1.8%; -1.7%) for the 20*t_C. The slight increase in error in the latter model is expected as the average value of 20*t_C for these wells is around 72 hours implying a greater extrapolation. Combining the calculated uncertainty in predicted T_{eq} for these models with that determined for the SLEX temperatures (Chapter 4; Appendix 4) gives an uncertainty in percentage accuracy of +2.1; -2.0% for the 50 hour extrapolation and +2.4; -2.3% for the 20*t_C. For the SLEX temperatures this implies a mean overall prediction accuracy range of between 0.2 and –3.9% in the fifty hour model and, 2.0 and –2.7% in the 20*t_C. For FTEX temperatures the equivalent ranges of uncertainty are likely to be larger although this is difficult to quantify.

Whilst the error envelope shown in Figure 7.8 accounts for systematic error in the input parameters of the semi-log plot, there still remains a question regarding the potential uncertainty in the chosen extrapolation time. In the case of an arbitrarily assigned extrapolation time, such as the 50 hour model, it is difficult to determine a basis upon which such uncertainty may be assigned. This is not the case in the 20*t_C model however where error estimates for circulation time are available. Average error in t_C for the forty-nine three data-point wells is equivalent to a range in extrapolation time of between 35 and 120 hours. Taking into account the effects of uncertainty in t_L and BHT this implies an average error in predicted temperature of +9.0°C; -10.6°C (+7.0%; -7.8%) and amounts to an uncertainty in percentage accuracy of +7.6; -8.4% relative to the SLEX. Such an error is not inconsiderable and once again highlights the importance of reliable assignation of extrapolation time.

7.7 Sensitivity Analysis

The use of both arbitrary and individual tailored extrapolation times in the semi-log plot appears to produce relatively unbiased temperature predictions for the available Cooper Basin wells. The apparent success of the arbitrary approach is something of a

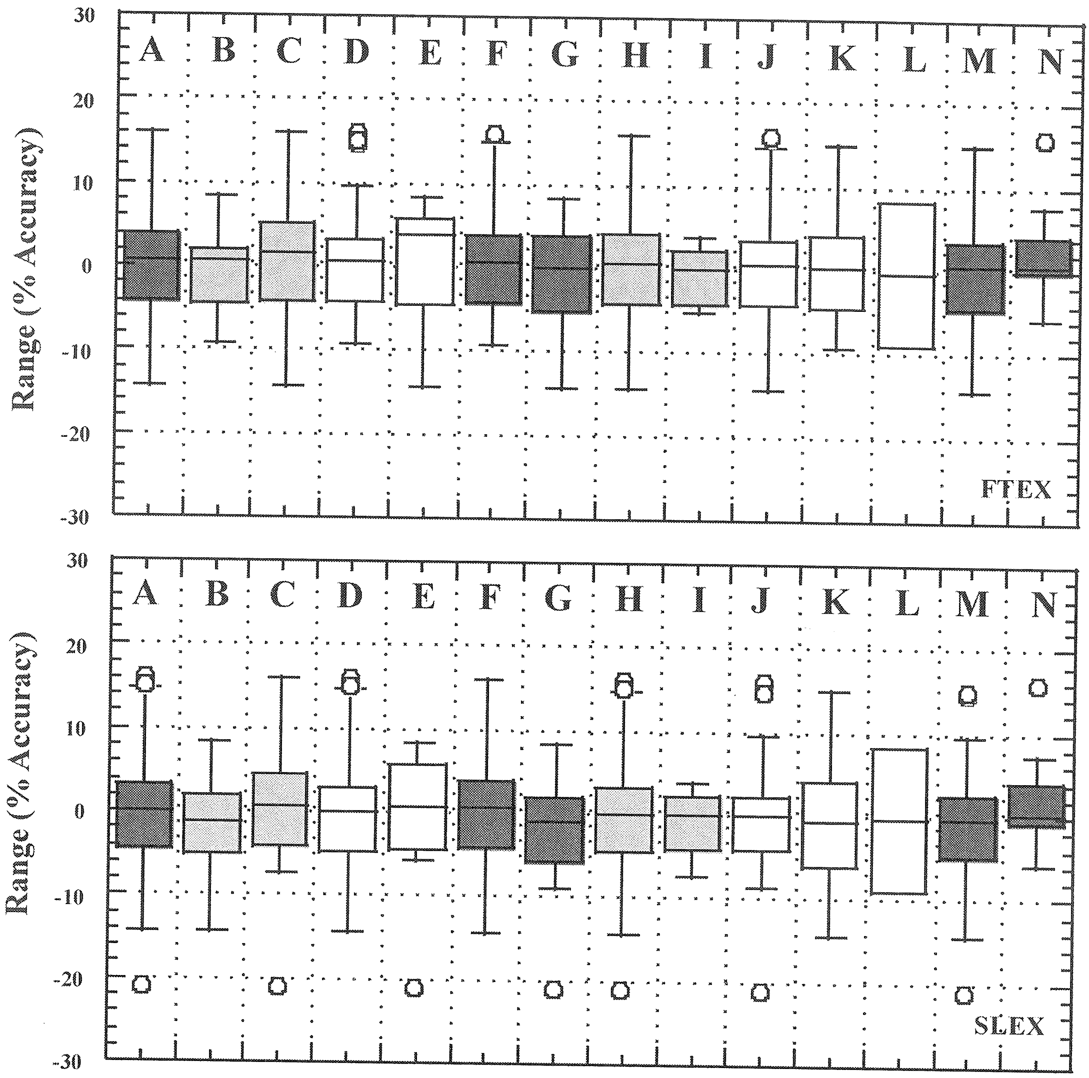

Figure 7.9: Box plots showing population distribution of results of semi-log plot formation temperature prediction accuracy from extrapolation to twenty times known circulation time relative to FTEX (top) and SLEX (bottom) static temperatures. In both cases, (**A**) is total population (n = 58); (**B**) subset of wells with statistically non-significant regressions (failure of regression F-test; n = 30); (**C**) subset of wells with statistically significant regressions (n = 28); (**D**) subset of wells with CBL category 1 (n = 47); (**E**) subset of wells with CBL category 2 (n = 11); (**F**) subset of wells with no coal bearing formations between CBL and BHT depth (n = 39); (**G**) subset of wells with coal bearing formations between CBL and BHT depth (n = 19); (**H**) subset of wells with three BHT data points only (n = 49); (**I**) subset of wells with four or more BHT data points (n = 9); (**J**) subset of wells with type 1 curves (n = 41); (**K**) subset of wells with type 2 curves (n = 15); (**L**) subset of wells with type 3 curves (n = 2); (**M**) subset of wells with only one recorded pre-logging conditioning episode (n = 49); (**N**) subset of wells with two or more recorded pre-logging conditioning episodes (n = 9).

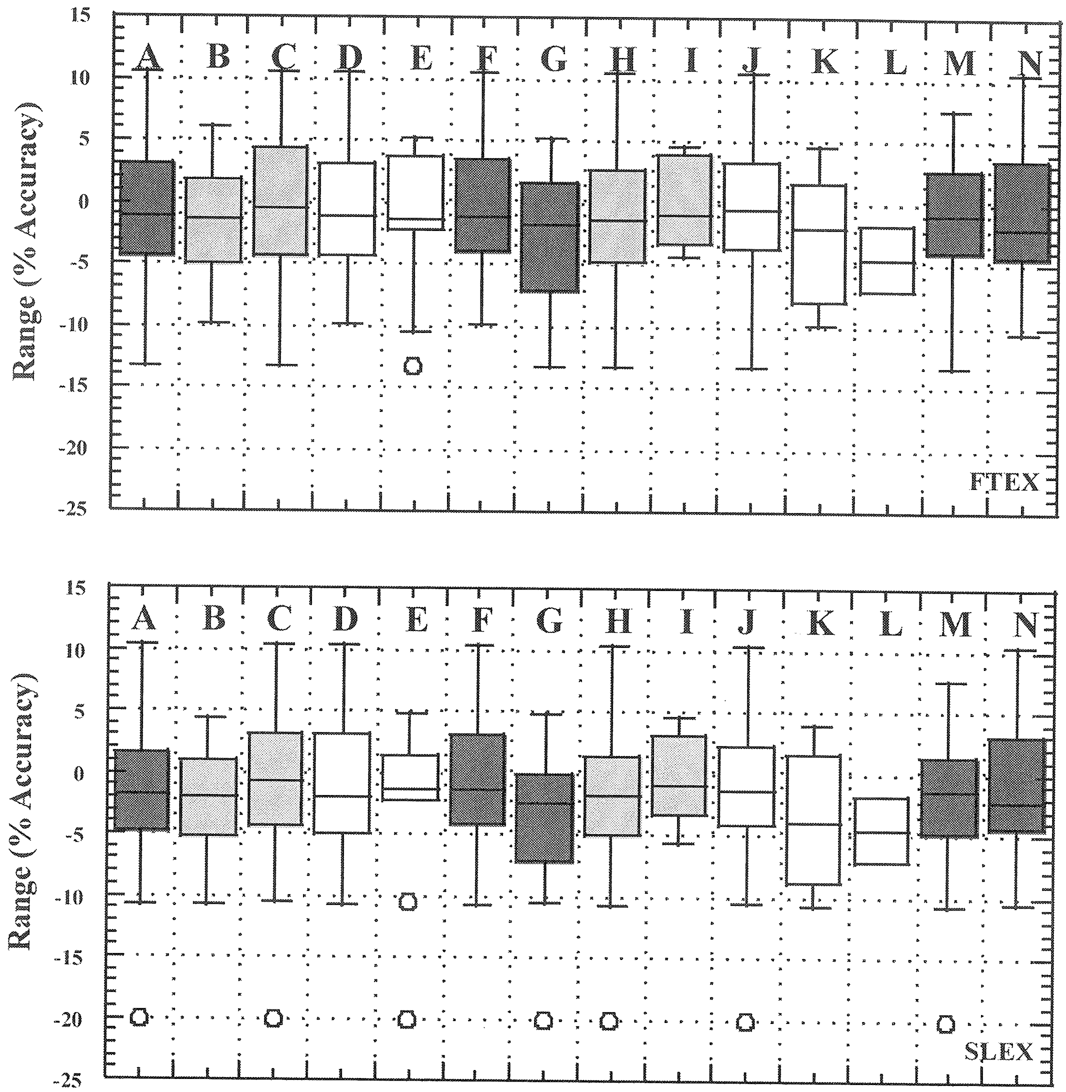

Figure 7.10: Box plots showing population distribution of results of semi-log plot formation temperature prediction accuracy from extrapolation to fifty hours relative to FTEX (top) and SLEX (bottom) static temperatures. In both cases, (**A**) is total population (n = 58); (**B**) subset of wells with statistically non-significant regressions (failure of regression F-test; n = 30); (**C**) subset of wells with statistically significant regressions (n = 28); (**D**) subset of wells with CBL category 1 (n = 47); (**E**) subset of wells with CBL category 2 (n = 11); (**F**) subset of wells with no coal bearing formations between CBL and BHT depth (n = 39); (**G**) subset of wells with coal bearing formations between CBL and BHT depth (n = 19); (**H**) subset of wells with three BHT data points only (n = 49); (**I**) subset of wells with four or more BHT data points (n = 9); (**J**) subset of wells with type 1 curves (n = 41); (**K**) subset of wells with type 2 curves (n = 15); (**L**) subset of wells with type 3 curves (n = 2); (**M**) subset of wells with only one recorded pre-logging conditioning episode (n = 49); (**N**) subset of wells with two or more recorded pre-logging conditioning episodes (n = 9).

surprise however, given the large range in calculated ideal extrapolation times which indicates that a one-size-fits-all solution should not really be ideal (Figure 7.5). In order to understand what factors (if any) may be controlling the accuracy of semi-log results, prediction quality must be compared to a number of parameters. Standard box-plots of semi-log plot result accuracy split along the factors identified in Chapter 4 are provided in Figures 7.9 and 7.10 for the 20*t_C and for 50 hour solutions respectively. Included within each of these figures are plots for results derived from statistically significant and non-significant regressions. A breakdown of statistically significant wells versus curve type and number of data points is given in Figure 7.11. Also provided in Figures 7.12 and 7.13 are a series of scatter plots representing prediction accuracy for both solutions versus input parameters, model fit (R^2), CBL extrapolation distance, CBL lag time, t_C and the ratio t_{L1}/t_C.

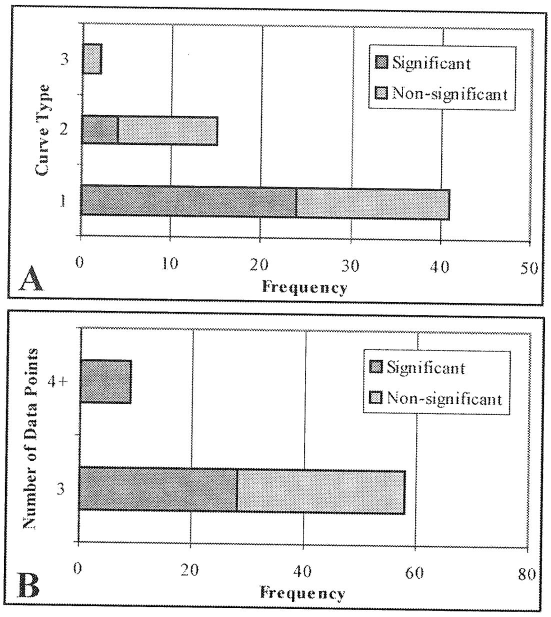

Figure 7.11: Bar graphs illustrating the relationship between the statistical significance of semi-log plot regression and (A) curve type; (B) number of available data points.

Examinations of the box-plot results depicted in Figures 7.9 and 10 provide relatively few clues as to the controls on semi-log model prediction accuracy. In both cases there is little variation between individual plots, the 20*t_C extrapolation in particular is remarkably uniform across all population groupings. In the case of the 50 hour solution there are some small variations, most notably an indication that result quality may deteriorate with curve type. Intriguingly, those variations which are evident in the 50 hour model are once again compatible with those first observed in the Horner and DMZC population distributions. Here also is a strong correlation between the quality of the model curve fit and curve type, with the majority of statistically significant regressions corresponding to type 1 curves (Figure 7.11). As always there is no obvious correlation between the significance of regression and result accuracy however, a fact confirmed by the scatter graphs of R^2 in Figures 7.12 and 7.13.

The nature of the controls governing prediction accuracy become more apparent upon examination of the scatter graphs provided in Figures 7.12 and 7.13. Once again there is evidence of a relationship between model prediction accuracy and the length of total t_L and total lag window. For the $20*t_C$ extrapolation the range of prediction accuracy is reduced to within ±5% of both static temperature estimates in most wells with total t_L >20 hours and lag window >15 hours. Similar patterns are also evident in the 50 hour data but are slightly less well defined. Once again, the only exceptions to these trends are the wells Woolkina 2 for both FTEX and SLEX static temperature and Ulandi 2 for SLEX temperatures. That increased total t_L should improve semi-log plot prediction quality is a reasonable finding, given that it implies both a stronger control on curve shape and a decrease in the extrapolation distance needed to determine T_{eq}. A further correlation evident in the $20*t_C$ model between the total length of t_C and accuracy again reflects the influence of extrapolation time upon the magnitude of a given prediction.

It would seem then that, like the two theoretical models, wells with long lag times are likely to produce more accurate formation temperature predictions when corrected using the semi-log plot. Unlike the Horner and DMZC models however, which both appear to chronically under-predict T_{eq} at short lag times, short lag time predictions produced by the semi-log plot appear to be relatively unbiased. The major control upon the accuracy of these predictions in fact appears to be the gradient, *m* of the fitted regression line (Figure 7.14). It is clear from this figure that strong over-prediction of T_{eq} is associated with steep regression gradients whilst under-prediction is often related to shallow gradients. For a $20*t_C$ extrapolation of CBST data, regression lines with gradients less than around 15 appear likely to produce an under-

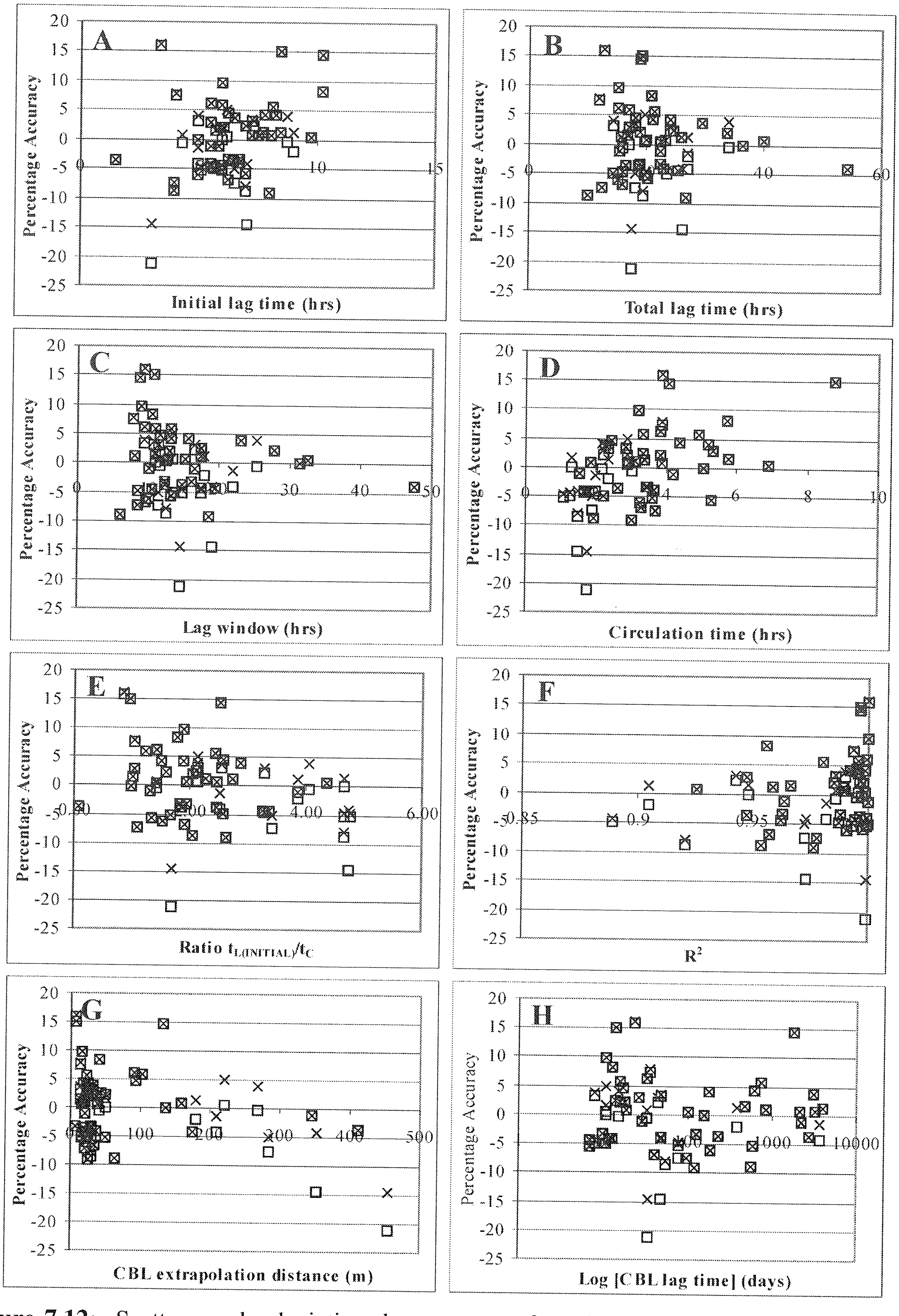

Figure 7.12: Scatter graphs depicting the accuracy of semi-log plot formation temperature prediction when extrapolated to twenty times the known circulation time as a percentage difference from estimated SLEX (squares) and FTEX (crosses) static temperature for 58 CBST wells versus (**A**) initial BHT lag time; (**B**) final BHT lag time (total lag time); (**C**) lag window (final – initial lag times); (**D**) total circulation time; (**E**) the ratio of initial lag time to total circulation time; (**F**) model fit (R^2); (**G**) the extrapolation distance of the CBL temperature and (**H**) the CBL lag time.

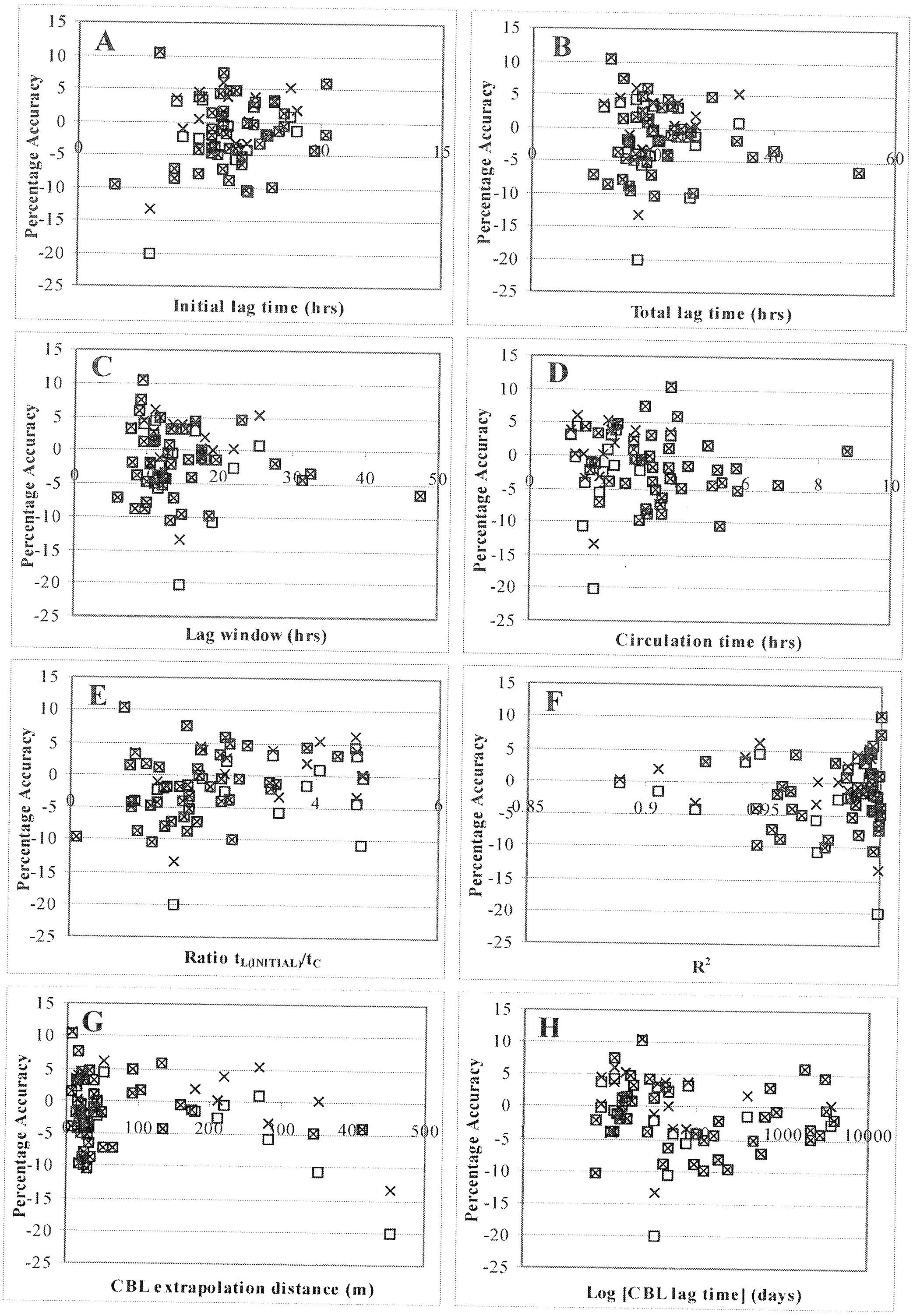

Figure 7.13: Scatter graphs depicting the accuracy of semi-log plot formation temperature prediction when extrapolated to fifty hours as a percentage difference from estimated SLEX (squares) and FTEX (crosses) static temperature for 58 CBST wells versus (**A**) initial BHT lag time; (**B**) final BHT lag time (total lag time); (**C**) lag window (final – initial lag times); (**D**) total circulation time; (**E**) the ratio of initial lag time to total circulation time; (**F**) model fit (R^2); (**G**) the extrapolation distance of the CBL temperature and (**H**) the CBL lag time.

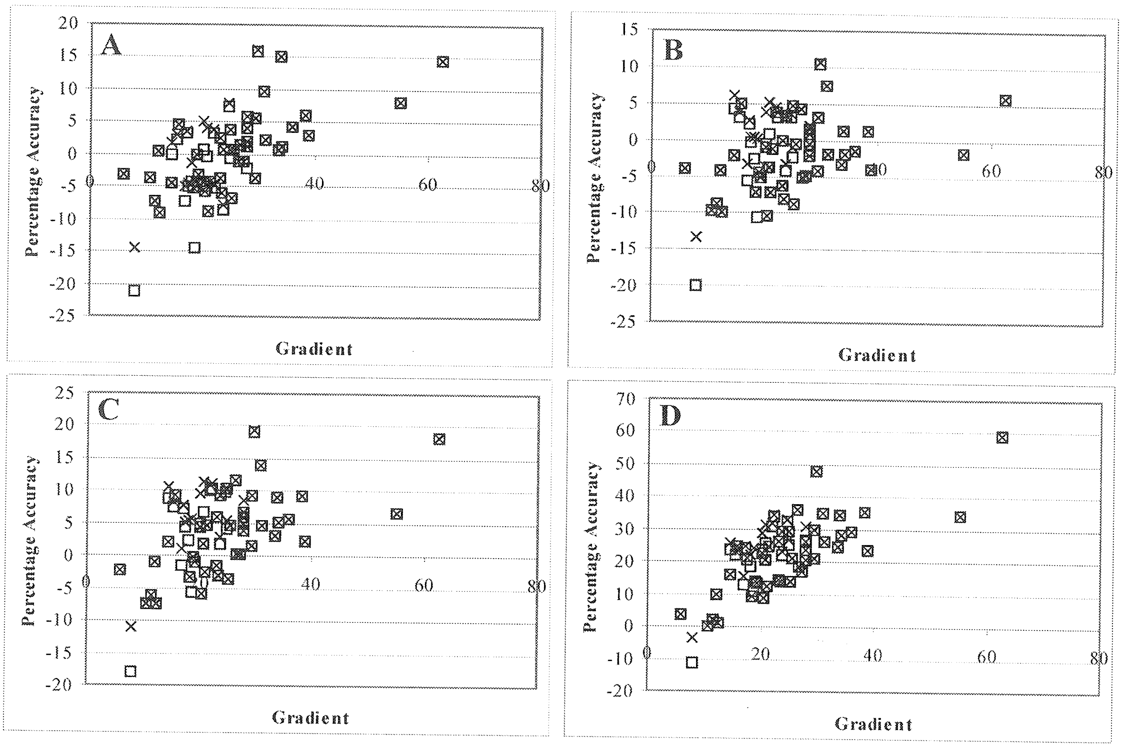

Figure 7.14: Scatter graphs depicting the accuracy of semi-log plot formation temperature prediction as a percentage difference from estimated SLEX (squares) and FTEX (crosses) static temperature for 58 CBST wells versus the gradient of the fitted linear regression for (**A**) extrapolation to twenty times the known circulation time; (**B**) extrapolation to 50 hours; (**C**) extrapolation to 100 hours and (**D**) extrapolation to 1000 hours.

prediction of static temperature whilst those with gradients over 30 should over-predict. Increasing the length of extrapolation time from 50 to 100 and 1000 hours serves to emphasise this correlation. Given the simple nature of the model this relationship is intuitively sensible and may provide a useful qualitative basis for the discrimination of semi-log plot results for short lag-time data. These results will be discussed in further detail in Chapter 9.

CHAPTER 8

TESTING THE EXPONENTIAL MODEL

8.1 Introduction

In many ways the ideal shape of a borehole temperature recovery curve is similar in form to that produced by a negative exponential $-e^{-x}$. It is this observation upon which the empirical Exponential model is based. As discussed previously in Chapter 3 all known exponential models are essentially variations on the form originally described in equation (4) by Nakaya (1953). For the purpose of this study it was decided to use the modified form of Perrier & Raiga-Clemenceau (1984) provided in equation (5) which is effectively identical to that of equation (4) but which substitutes ($T_{eq} - T_m$) for the constant *A* and α for the constant *b*.

8.2 Determination of –α

Input parameters required for equation (5) are limited to BHT and lag time (t_L) data. In order to solve for T_{eq} it is necessary to undertake a curve matching exercise for the exponential equation on a graph of BHT versus t_L. Initial attempts at accomplishing this with conventional graphical software failed however, the programs were unable to optimise the unknown exponential constant (–α). To overcome this problem the method of Parasnis (1971) was used to manually optimise α from known BHT data prior to attempting the curve matching exercise. Differentiating equation (5) by time Parasnis (1971) produces the equation:

$$\frac{dT}{dt} = (T_f - T_m)\alpha e^{(-\alpha t)} \qquad (34)$$

Assigning $(dT/dt)_1$ and $(dT/dt)_2$ to be the rates of change at time $t = t_1$ and $t = t_2$ and rearranging gives:

$$\ln\frac{(dT/dt)_2}{(dT/dt)_1} = -\alpha(t_2 - t_1) \qquad (35)$$

Using (35) it was possible to solve for -α by determining the gradient of a linear regression on a semi-log plot of ΔT/Δt versus time. Values of ΔT/Δt were determined for consecutive sets of BHT temperature and were assigned values of t equal to the mid-point of the equivalent lag time interval. Examples of the resulting graphical solutions for -α are presented in Figure 8.1.

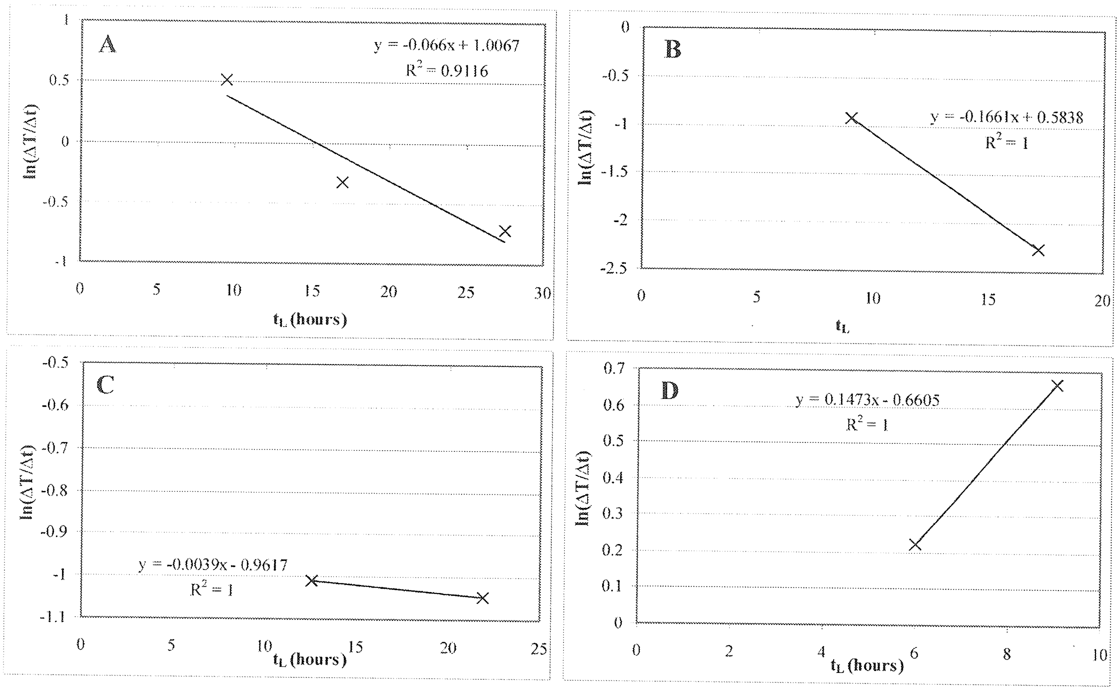

Figure 8.1: Typical examples of the graphical determination of the exponential constant –α using the method of Parasnis (1971). –α is given by the gradient of the regression lines. Note the reversal of gradient associated with the type 3 curve (D). (A) Bookabourdie 2 (SLEX = 144.3); (B) Taloola 2 (SLEX = 104.2); (C) Woolkina 2 (SLEX = 148.8) and (D) Della 10 (SLEX = 138.1). Refer to Figure 4.6 for comparison with the primary temperature-time data curves.

The fit of model curves generated from values of –α determined using the method of Parasnis (1971) were generally quite good with an average R^2 = 0.9973 for 61 wells. It is evident from Figure 8.1 however that graded wells with only three available BHT generate only two points from which to determine –α. For these wells the uncertainty in regression is likely to be high implying that the corresponding estimates of –α may vary significantly from the optimum. The existence of non-ideal estimates of –α was demonstrated for the well Spencer 3 where the value determined, 0.1198, produced an exponential curve which fitted the temperature-time data with an R^2 = 0.99846. Varying $-\alpha$ slightly above and below this figure it was found that substituting a value of 0.1360 resulted in a curve with a perfect fit of $R^2 = 1$. Clearly, the values of $-\alpha$ determined by Parasnis's method are close to, but not necessarily the same as, the most ideal choice. In the case of Spencer 3 the difference between the calculated and ideal $-\alpha$ amounted to a difference of 0.5°C in predicted T_{eq} although the ideal fit actually produced a worse prediction when compared to the known static temperature.

In addition to the problem of idealising the curve fit was the fact that, as yet, no evidence existed that the value of $-\alpha$ generated by the method of Parasnis (1971) was exclusive. It was possible that there may be other optimal domains of $-\alpha$ which were not detected by this approach. In order to resolve these problems it was necessary to conduct a full non-linear regression of the exponential equation using a more sophisticated software system. To meet this need a MATLAB M-file previously created by Dr Prame Chopra was adapted (by Dr Chopra) to perform non-linear regression of the Exponential equation. Renamed EXP2 the M-file offers a choice of seven search algorithms and two line search methods and optimises curve fit via a least-squares technique. The program relies upon an initial user-provided set of function constants as a starting point for iteration. In this case the estimates used were those previously determined by the method of Parasnis (1971) described above.

Tests of the 12 different combinations of search algorithm and line search methods available in EXP2 were undertaken on three different wells. In each case curve fits were found to be identical irrespective of the technique used. For all remaining data solutions were generated using Gauss-Newton regression with mixed polynomial interpolation. To determine whether these solutions were unique, results from four wells were re-calculated using sets of arbitrary input parameters above and below those of the Paranis (1971) solution. In all cases successfully fitted solutions were found to be identical. It appeared however that there were limits to the magnitude of input estimates. Combinations which were either too large or too small produced a failure whereby the program was only able to fit a straight line.

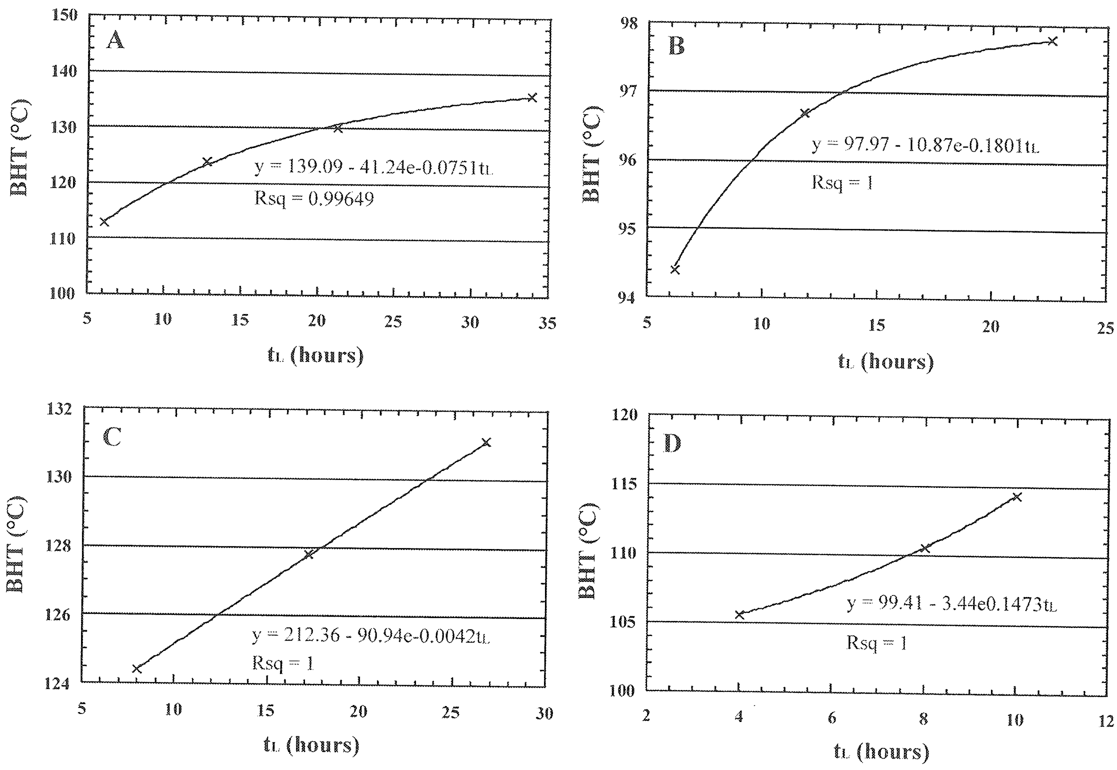

Figure 8.2: Typical examples of exponential model curve fits as generated by EXP2. Predicted equilibrium temperature is given by the first constant term. Note the differences in the shape of the fitted curve between the type 1 curves (A & B) and the type 2 (C) and 3 curves (D). (A) Bookabourdie 2 (SLEX = 144.3); (B) Taloola 2 (SLEX = 104.2); (C) Woolkina 2 (SLEX = 148.8) and (D) Della 10 (SLEX = 138.1). Refer to Figure 4.6 for comparison with the primary temperature-time data curves.

8.3 Application of the Exponential Model

Graphical representations of the predicted EXP2 exponential curve fits are presented in Figure 8.2. Of all the BHT recovery models examined, the empirical exponential was the only one that was capable of fitting exactly to a Type 3 or concave up temperature-time curve. In these cases the calculated exponential power was positive and the resulting temperature build-up curves tended to infinity with increasing lag time. In all, five wells were affected by this problem including the three identified Type 3 wells, Big Lake 35, Della 10 and Spencer 5 as well as two additional Type 2 wells, Big Lake 32 and Toolachee 19. The occurrence of this behaviour in Type 2 wells, for which the temperature-time curve is considered to approximate a straight line (linear regression $R^2 > 0.99$), is a reflection of the sensitivity of the exponential fit. As the modelled behaviour of these wells was physically impossible they were excluded from further consideration.

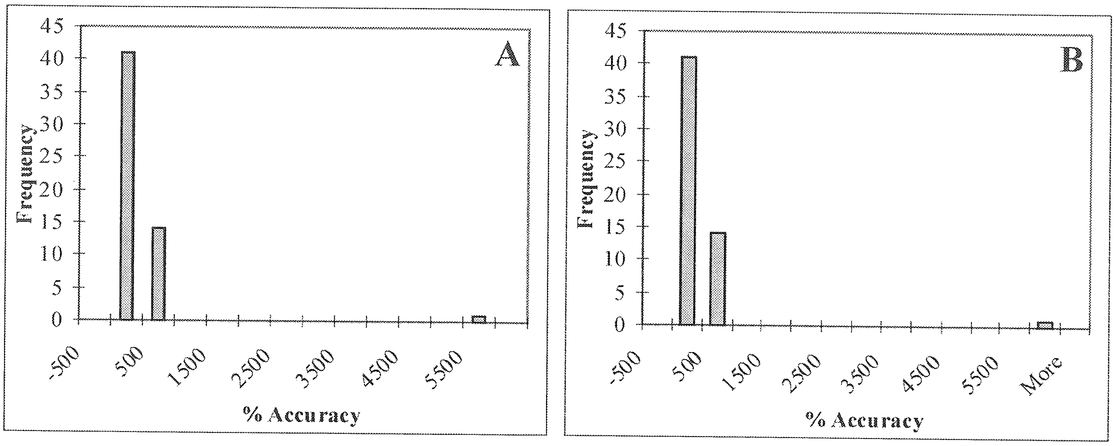

Figure 8.3: Results of exponential model formation temperature prediction from fifty-six (56) CBST wells. Accuracy is calculated relative to the known static formation temperature, positive numbers indicate percentage over-prediction, negative percentage under-prediction. In graph (**A**) static temperatures are all straight line extrapolated (SLEX), in (**B**) formation compensated static temperatures (FTEX) are used where available.

8.4 Model Results

At 0.9984 the average value of R^2 for the fifty-six remaining exponential curve fits was the highest of all the tested BHT recovery models. The great majority of wells recorded a perfect fit ($R^2 = 1$) and the worst recorded fit was that of well Narcoonowie 3 with $R^2 = 0.9524$ ($n = 6$). Figure 8.3 presents a histogram of the results of exponential formation temperature prediction accuracy relative to the FTEX for the 56 modelled wells. Clearly there is a problem with this distribution - a single temperature prediction has returned the outlandish value of +5737.3% relative to the known static. The well concerned, Ulandi 2, is a Type 2 curve for which a linear temperature-time regression returns a perfect fit. It would appear that the flexibility of the exponential model has enabled a close fit to this data, calculating a near straight-line regression with a value of $-\alpha$ equal to 0.0001. Examination of other results reveal two additional wells in which a similar, albeit somewhat less extreme, pattern is visible. Pondrinie 5 and Woolkina 2 are also both Type 2 curves for which straight-line regression on a temperature-time plot gives a fit of $R^2 \geq 0.9998$. Each of these wells is characterised by both $-\alpha < 0.01$ and T_{eq} which is over-estimated by >40% relative to the FTEX. The repeated identification of temperature predictions from Woolkina 2 and Ulandi 2 as outliers to the broader result population strongly implies that there may be some form of as-yet unidentified bias affecting these wells. Whilst there are numerous other wells which are Type 2 curves, it is only these which are consistently singled out, regardless of the model with which they are treated. In this case it appears that the predictive capacity of the exponential model is strongly dependent upon the quality of the input data, much more so than the other models tested. As the modelled behaviour of these three wells is physically unrealistic they were excluded from further consideration. The average R^2 of the remaining 53 wells was 0.9983.

	SLEX	FTEX
Mean	-3.5	-2.8
Standard Error	1.2	1.1
Median	-4.4	-4.0
Standard Deviation	8.5	8.1
Sample Variance	71.7	65.9
Kurtosis	1.6	1.6
Skewness	0.8	1.2
Range	43.5	37.6
Minimum	-21.8	-15.3
Maximum	21.6	22.3
Count	53.0	53.0
Confidence Level (95.0%)	2.3	2.2

Table 8.1: Standard descriptive statistics for the histogram distributions of Exponential model results given in Figure 8.4.

Histogram distributions of prediction accuracy for the 53 remaining exponential model formation temperature estimations are presented in Figure 8.4. Standard descriptive statistics for these distributions are included in Table 8.1 (above). Overall, the results of the exponential modelling are disappointing relative to those of Hermanrud *et al.* (1990; Table 3.1) who found this model to be biased but relatively precise. In this case, both SLEX and FTEX results are observed to be biased toward under-prediction whilst the standard deviation of the model results is the highest of all models examined so far. Despite the bias toward under-prediction both sets of data are found to be significantly skewed to the right and for the first time a FTEX result population is less normal than the SLEX (Figure 8.5). In addition to the skew both populations are also observed to have a significant positive kurtosis.

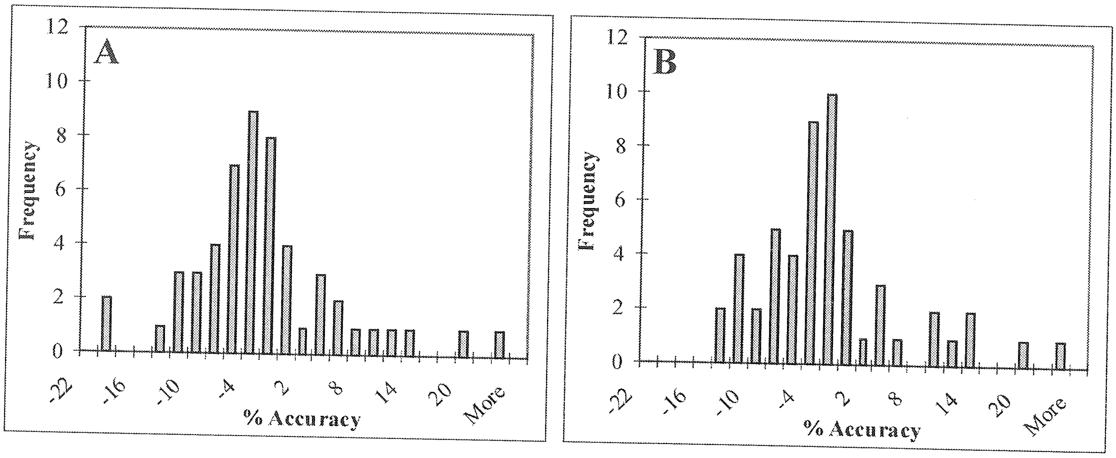

Figure 8.4: Results of exponential model formation temperature prediction from fifty-three (53) CBST wells. Accuracy is calculated relative to the known static formation temperature, positive numbers indicate percentage over-prediction, negative percentage under-prediction. In graph (**A**) static temperatures are all straight line extrapolated (SLEX), in (**B**) formation compensated static temperatures (FTEX) are used where available.

8.5 Statistical Analysis

The non-linear nature of the regression used in the exponential curve-fitting implies that the methods of assessing statistical significance used for other models do not apply here. This situation is further complicated by the fact that neither the SLEX nor FTEX result populations are normally distributed. Of the fifty-three (53) wells included in the final result population forty-four (44) are characterised by a perfect curve fit ($R^2 = 1$). Such strong correlations should imply small statistical uncertainty yet they obviously do not correspond to perfect temperature prediction. Once again it appears that the goodness of model fit is not an indicator of the likely prediction accuracy. It is interesting, and no doubt highly significant however, that all nine (9) wells with curve fits of $R^2 < 1$ are characterised by four or more temperature data points. Such a result implies that the apparent goodness of model fit to most data curves is probably deceptive, the equivalent of fitting a straight line to only two data points.

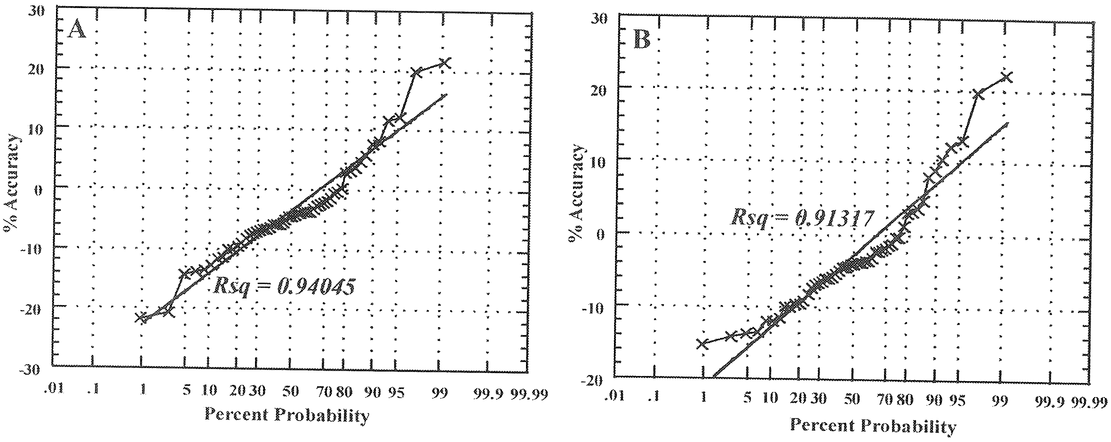

Figure 8.5: Normal probability plots for distribution of exponential model formation temperature prediction accuracy relative to (**A**) SLEX static temperatures and (**B**) FTEX static temperatures. Crosses represent location of individual data points. *Rsq* refers to the fit of the linear regression.

8.6 Systematic Uncertainty

As for the semi-log plot, systematic uncertainty in the exponential model is derived entirely from resolution limits on the primary input parameters lag time and BHT. The magnitude of this uncertainty is illustrated in Figure 8.6 where both x (t_L) and y (BHT) error bars are included for each data point. As the error in both directions is independent it is possible to estimate potential systematic uncertainty by use of an error envelope. For three-point wells this was a relatively simple exercise, average error in the forty-four available data sets calculated as +11.3°C; -3.0°C (+7.8%; -2.2%). The apparent bias of error in the positive direction is explained by the existence of several cases in which the magnitude of estimated error in the positive direction was greatly exaggerated compared to that in the negative. The cause of this behaviour appeared to be variations in the curvature of the upper and lower limits of the error envelope. Strong positive error was once again associated with curves which were a closer approximation to a straight line. Hence the well Brolga 3 was characterised by an error envelope of +183.2%; -14.7%, corresponding to curves where $-\alpha$ equals 0.0031 and 0.0651 respectively.

Combining the calculated uncertainty in predicted T_{eq} with that determined for the SLEX temperatures (Chapter 4; Appendix 4) gave a total uncertainty in percentage accuracy of +9.0; -2.9%. For the SLEX temperatures this implies a mean overall prediction accuracy range of between 5.5 and –6.4%. For FTEX temperatures the equivalent range of uncertainty is likely to be larger although this is difficult to quantify.

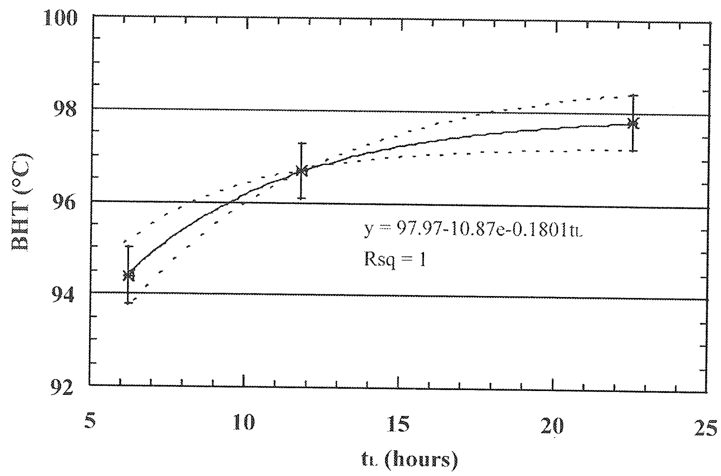

Figure 8.6: Error envelope determined for a typical three-point exponential model regression in well Taloola 2. Independent error in x (t_L) and y (BHT) directions are indicated by error bars. The solid regression line indicates the best fit solution as shown in Figure 8.2. The dotted regression lines indicate the extents of the calculated error envelope.

8.7 Sensitivity Analysis

It is clear from Figure 8.4 that the results of exponential model temperature prediction accuracy are distributed in an unusual way. In spite of an average indicating bias toward under-prediction, both SLEX and FTEX populations are significantly skewed to the right, towards over-prediction. The likely cause of this behaviour has already been discussed in preceding sections where it was found that over-prediction by the exponential model was related to the degree of curvature or "shape" of the temperature-time curve. In order to determine the strength of this relationship, and to investigate the possibility that other parameters may also be influencing model outcomes, the sensitivity of model prediction accuracy to a number of factors must be investigated. To this end, standard box-plots of model result accuracy split along the factors identified in Chapter 4 are provided in Figure 8.7. Also, in Figure 8.8, a series of scatter plots representing model prediction versus both initial and total lag time, total lag window, model fit R^2, CBL extrapolation distance, CBL lag time, total circulation time, the ratio t_{L1}/t_C and the magnitude of the exponential constant $-\alpha$ are presented.

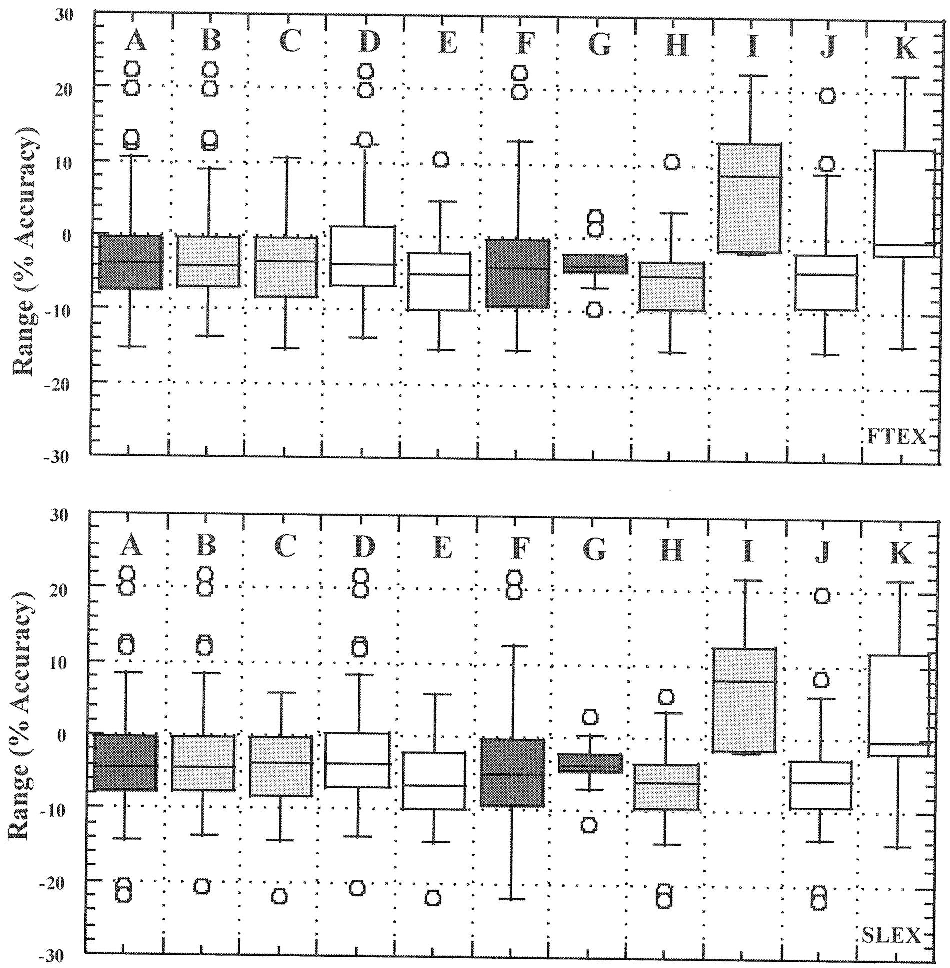

Figure 8.7: Box plots showing population distribution of results of exponential model formation temperature prediction accuracy relative to FTEX (top) and SLEX (bottom) static temperatures. (**A**) total population (n = 53); (**B**) subset of wells with CBL category 1 (n = 42); (**C**) subset of wells with CBL category 2 (n = 11); (**D**) subset of wells with no coal bearing formations between CBL and BHT depth (n = 35); (**E**) subset of wells with coal bearing formations between CBL and BHT depth (n = 18); (**F**) subset of wells with three BHT data points only (n = 44); (**G**) subset of wells with four or more BHT data points (n = 9); (**H**) subset of wells with type 1 curves (n = 43); (**I**) subset of wells with type 2 curves (n = 10); (**J**) subset of wells with only one recorded pre-logging conditioning episode (n = 44); (**K**) subset of wells with two or more recorded pre-logging conditioning episodes (n = 9).

It is immediately apparent from the box plots of Figure 8.7 that there are two stand-out sub-population groupings within the exponential model results. The range of prediction accuracy from wells characterised by Type 2 curves accounts for all of the most extreme temperature over-estimations. Similarly, prediction from those wells which have recorded two or more pre-logging conditioning episodes are also exceptionally high. The former observation may be directly accredited to curve shape, Type 2 curves are near-straight lines for which an exponential fit will inevitably result in over-prediction. In the latter case, six out of nine wells with multiple pre-logging conditioning episodes are in fact Type 2 curves, implying that much of the extreme over-prediction within this population is related to curve shape. This raises the interesting possibility of a causative relationship between the use of extra circulation in a well and the shape of the temperature-time curve. Increasing circulation time should cause a deeper penetration of the thermal anomaly into the formation. This would in turn decrease the radial temperature gradient at the well wall, slowing the initial recovery. It is conceivable that this effect could produce a visible flattening of the temperature-time curve such that, at relatively short lag times, it takes on the appearance of a straight line (Figure 4.6). Intriguingly however none of the three excluded wells, Ulandi 2, Woolkina 2 or Pondrinine 5 are noted as having experienced additional circulation.

The strength of the dependence of model prediction upon the degree of curvature in the fitted model is evident in the plot of $-\alpha$ versus percentage accuracy in Figure 8.8. For values of $-\alpha < 0.5$ there appears to be a strong relationship between decreasing $-\alpha$ (increasing linearity) and increasing over-prediction. As previously recognised, there exists a range of $-\alpha$ for which temperature prediction is unrealistic. At present the limit of this range has been set at $-\alpha < 0.01$. If this were to be extended to higher values it is apparent that the overall performance of the model in the remaining wells would be improved. Perhaps more significant, however, is the possibility that by using the value of $-\alpha$ determined for a given temperature vs. time curve it may be possible to qualitatively estimate where an individual exponential prediction will lie within the general CBST population distribution.

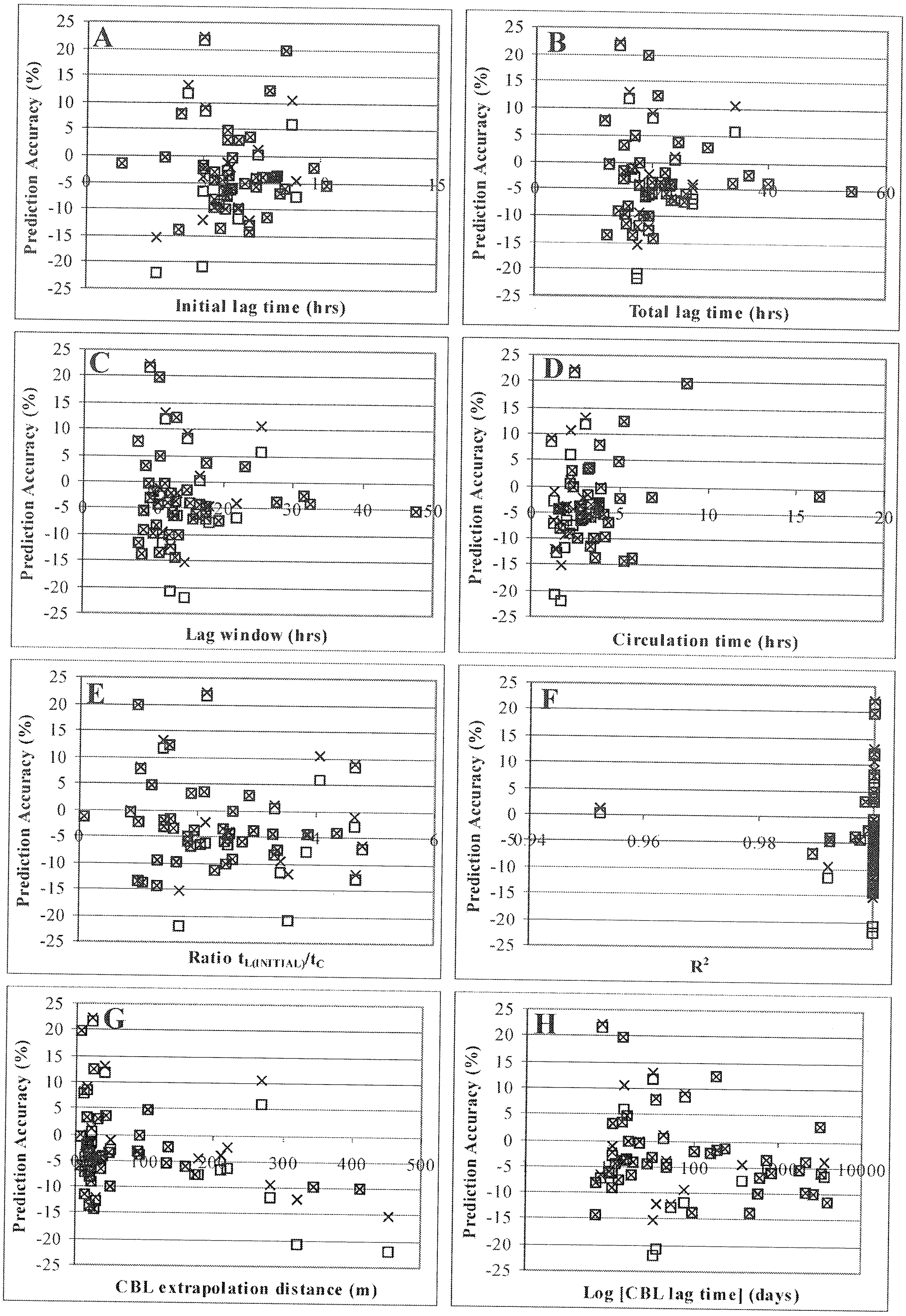

Figure 8.8: Scatter graphs depicting the accuracy of Exponential model formation temperature prediction as percentage difference from estimated SLEX (squares) and FTEX (crosses) static temperature for 53 CBST wells versus (**A**) initial BHT lag time; (**B**) final BHT lag time (total lag time); (**C**) lag window (final – initial lag times); (**D**) total circulation time; (**E**) the ratio of initial lag time to total circulation time; (**F**) model fit (R^2); (**G**) the extrapolation distance of the CBL temperature (**H**) the CBL lag time and (**I**) the exponential constant alpha (α).

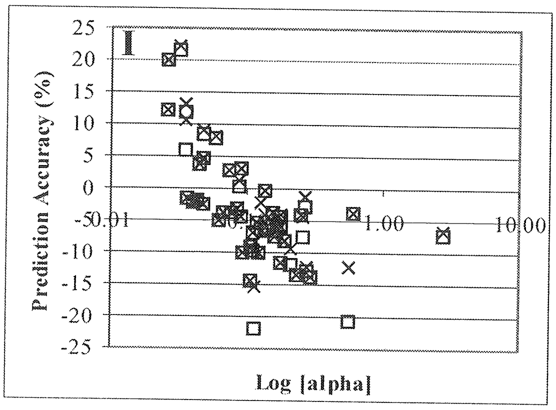

Figure 8.8: Scatter graphs depicting the accuracy of Exponential model formation temperature prediction as percentage difference from estimated SLEX (squares) and FTEX (crosses) static temperature for 53 CBST wells versus (**A**) initial BHT lag time; (**B**) final BHT lag time (total lag time); (**C**) lag window (final – initial lag times); (**D**) total circulation time; (**E**) the ratio of initial lag time to total circulation time; (**F**) model fit (R^2); (**G**) the extrapolation distance of the CBL temperature (**H**) the CBL lag time and (**I**) the exponential constant alpha (α).

Aside from the strong relationship between prediction accuracy and $-\alpha$ there is relatively little correlation visible in the remaining scatter graphs of Figure 8.8. One possible exception is a weak correlation between result accuracy and both total lag time and lag window. With one exception (Sturt 1), exponential model predictions are improved to within around ±5% of both estimated values of true formation temperature when total lag time exceeds around 30 hours and/or the total lag window is greater than around 25 hours. As for the semi-log plot, such a result is probably not unexpected as a longer overall lag period should be characterised by a well defined data-curve, ensuring a fitted model that is a closer approximation to the long-term temperature-time recovery. These results, along with those of the previous three models, will be discussed further in the next chapter.

CHAPTER 9

CORRECTING COOPER BASIN DRILL TEMPERATURES

9.1 Introduction

In Chapters 5 - 8 the results of temperature prediction from four of the most common BHT recovery models were presented for a subset of 61 Cooper Basin wells in which the static temperature was already known. In each case models were successfully applied to a high proportion of the available database, generating a result population characterised by a distinct range of prediction accuracy. Studies of uncertainty in the predicted formation temperatures were presented from both a statistical and systematic (measurement) perspective. Analyses of the controls (if any) on model performance were also included in the final section "Sensitivity Analysis" of each model chapter. In the current chapter these model results will be compared and their relative performances assessed. The knowledge gained from this exercise will then be used, where possible, to make recommendations for both the collection of future Cooper Basin borehole temperature data and the use of existing temperature records. One important application of this knowledge is in the creation of a new, updated temperature map specifically for the Cooper Basin region.

9.2 Model Results

A summary of the results generated from BHT modelling of Cooper Basin wells in Chapters 5 - 8 is presented in Table 9.1 and graphically in Figure 9.1. A quick perusal of these data is sufficient to enable a number of conclusions to be drawn. Based on these data it would appear that in this instance most models are, on average, characterised by a bias towards under-prediction. Empirical models (semi-log plot; exponential) are, on average, more accurate than theoretical (Horner; DMZC) which collectively display the greatest negative bias. The ostensible mean accuracy of the empirical models comes at the expense of precision however and in all cases the standard deviations of these results are greater than those produced by the theoretical solutions. The populations of prediction accuracy generated by the different empirical

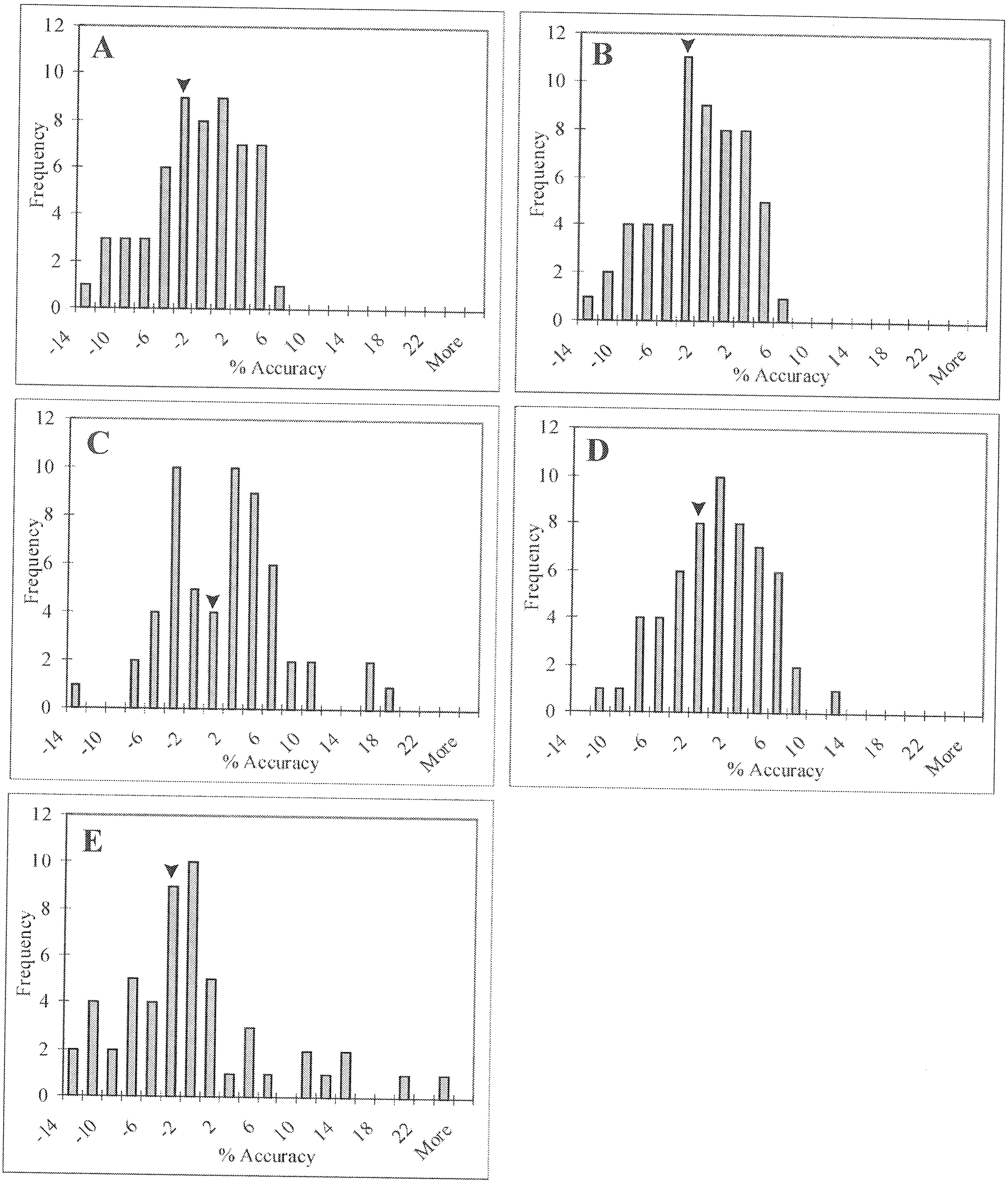

Figure 9.1: Histogram distributions of model temperature prediction accuracy relative to FTEX static temperatures as presented in Table 9.1 for (**A**) Horner Plot; (**B**) DMZC Model (Cooper & Jones, 1956); (**C**) Semi-log plot extrapolated to twenty times the known circulation time; (**D**) Semi-log plot extrapolated to 50 hours and (**E**) Exponential model. The marker indicates the location of the mean prediction accuracy.

models are also quite diverse, and contrast with the strong concurrence of results from the two theoretical models.

Model	Mean	σ	Max	Min	n
Horner Plot	-3.5	4.8	5.5	-15.6	57
DMZC (Cooper & Jones, 1959)	-3.7	4.7	5.5	-15.5	57
Semi-log plot x = 20*t_C	0.3	6.0	16.1	-14.5	58
Semi-log plot x = 50 hour	-1.2	5.0	10.6	-13.4	58
Exponential	-2.8	8.1	22.3	-15.3	53

Table 9.1: Summary of CBST BHT modelling results as percentage result accuracy versus FTEX static temperature. Positive numbers indicate percentage over-prediction and negative percentage under-prediction relative to the static temperature.

Evidence from the previous Chapters indicates that the apparent bias toward under-prediction evident in most models is likely to be real, there being no detectable impact from outside influences such as exothermic cement hydration. Some questions remain about the size of the actual bias however. Model results presented in Table 9.1 are those derived from the comparison of model T_{eq} and FTEX static temperatures. For much of the previous chapters FTEX or formation temperature corrected extrapolations of known CBL temperature were preferred to that of the SLEX or straight line extrapolations. This preference was based upon the apparent ability of the FTEX calculation to correct bias introduced into the SLEX by the presence of porous aquifers in the extrapolation interval. Failure to account for these units, which are known to be host to lower than average formation temperature gradients, implies that some SLEX are likely to be over-estimations of the true static temperature. The success of the FTEX correction in counteracting this bias was evident in the fact that most population distributions of model result accuracy relative to the SLEX were significantly skewed towards under-prediction (Table 9.2), while those with FTEX corrections were not.

Following completion of the modelling work, new temperature logs became available from the deep geothermal well Habanero 1 drilled at Innamincka in the Cooper Basin (Chapter 11). Like the AMS data derived from petroleum wells, temperature logs available from Habanero were not recorded under conditions of thermal equilibrium. Logs available from the new well do have significantly longer lag times than those of the AMS logs however, of the order of days rather than hours (Figure 11.2). Data available from these logs indicate that formation gradients in the Hutton and Namur

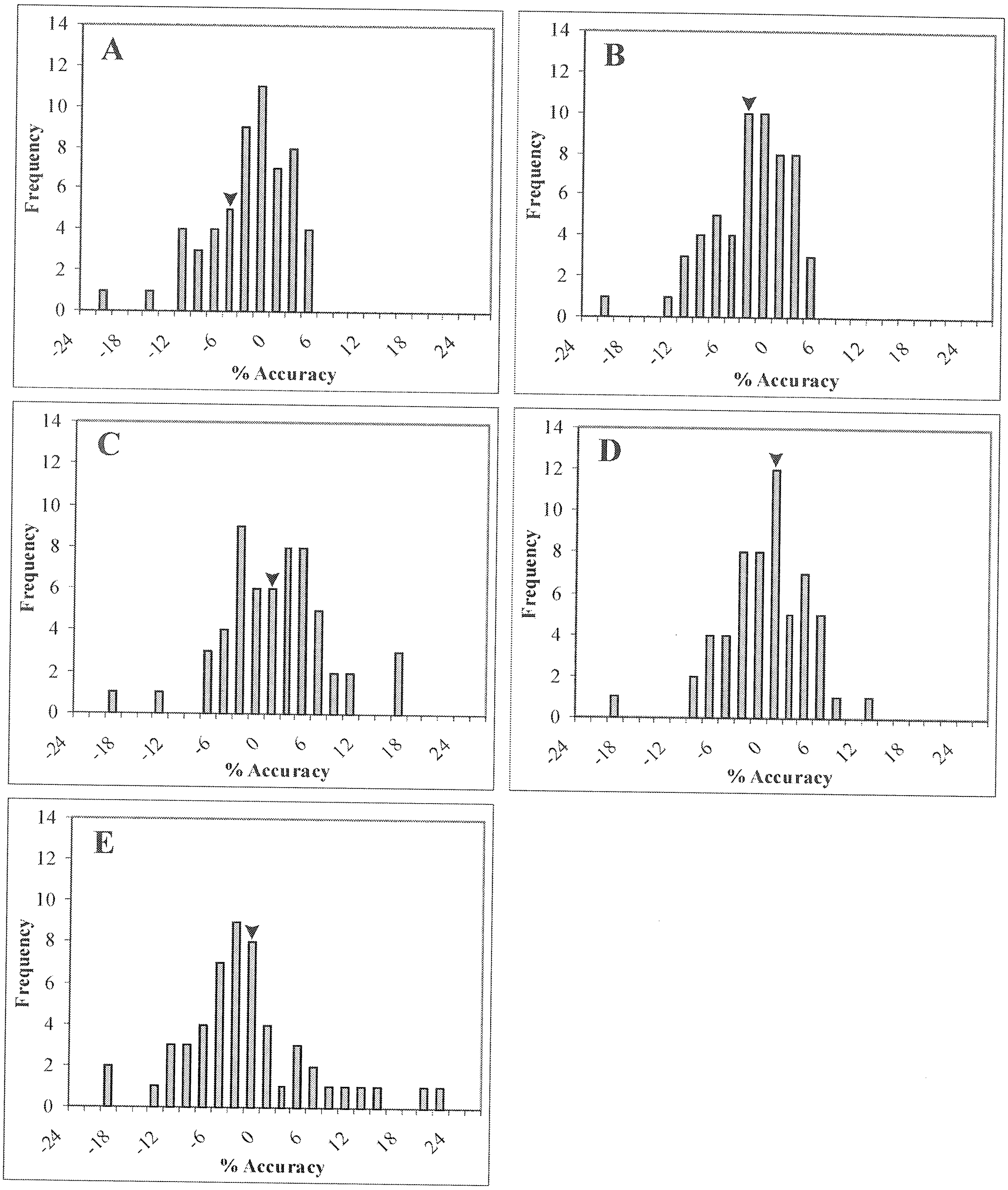

Figure 9.2: Histogram distributions of model temperature prediction accuracy relative to SLEX static temperatures as presented in Table 9.2 for (**A**) Horner Plot; (**B**) DMZC Model (Cooper & Jones, 1956); (**C**) Semi-log plot extrapolated to twenty times the known circulation time; (**D**) Semi-log plot extrapolated to 50 hours and (**E**) Exponential model. The marker indicates the location of the mean prediction accuracy.

aquifers within the Nappamerri Trough are higher by around 10ºC/km than those derived from the AMS data and used in the FTEX corrections. Whilst the Nappamerri Trough is known to be host to locally high heat flows (Chapter 10) and may not, therefore, be fully representative of the Cooper Basin as a whole, it does seem likely that the FTEX corrections used in the extrapolation of CBL temperatures may have been too low. As a consequence it is probable that the FTEX static temperatures themselves may be too low, implying that the apparent reduction of under-prediction associated with these results may be misleading. Increasing FTEX temperatures effectively brings the result population of model prediction accuracy for this static temperature towards that of the SLEX (Figure 9.2) implying that true model performance probably lies somewhere between these two extremes.

Model	Mean	σ	Max	Min	n
Horner Plot	-4.4	5.2	3.5	-22.2	57
DMZC (Cooper & Jones, 1959)	-4.6	5.1	3.6	-22.0	57
Semi-log plot x = 20*t_C	-0.4	6.6	15.9	-21.1	58
Semi-log plot x = 50 hour	-1.9	5.3	10.4	-20.1	58
Exponential	-3.5	8.5	21.6	-21.8	53

Table 9.2: Summary of CBST BHT modelling results as percentage result accuracy versus SLEX static temperature. Positive numbers indicate percentage over-prediction and negative percentage under-prediction relative to the static temperature.

9.3 Accuracy and Precision

In the preceding chapters a significant amount of space has been devoted to the assessment of both the statistical and systematic (measurement) uncertainties associated with the application of models for BHT correction to the CBST database. Whilst these two kinds of error analysis have some commonality they also differ as the results of this study clearly demonstrate. Here, analysis of measurement error typically predicted relatively small uncertainties that were often dwarfed by those forecast using statistical techniques. This divergence between statistical and systematic error analyses is of great significance to the interpretation of the BHT model results. Deciding which uncertainty best reflects true conditions will effectively determine the utility of applying these models to commercial well data.

Whilst it is possible to combine systematic or measurement error into linear regression (Fuller, 1987) this form of treatment is beyond the scope of this work. Instead, statistical and systematic error have herein been treated separately following the convention outlined by Cooper *et al.* (1992). The use of statistical techniques to estimate uncertainty in linear regression aims to assess the probability that the regression result may be influenced by random error. These techniques effectively place an outer limit on the probable configuration of the regression line based upon the size and distribution of the given data set. As most of the CBST wells used have five or less data points it is to be expected that the statistical uncertainty in regression will often be high and in most cases this is what is seen to happen (Table 9.3). It is also clear from these data that the calculated statistical uncertainty is highly variable both within and between individual model results. For any given model the statistical uncertainty was found to be greatest in those wells which failed the regression F-test. There was also a large disparity between different models (*e.g.* the Horner and DMZC), a product of the different mechanisms utilised by each solution. Nevertheless, in comparing results of Tables 9.1, 9.2 and 9.3 it becomes evident that, for all well types and all models, the magnitude of the average statistical uncertainty is greater than the average bias in prediction accuracy. In other words, the actual difference between predicted and true formation temperature is smaller than the statistical uncertainty of the prediction. This means that we cannot conclude with 95% confidence that there is, in fact, any bias at all in the model prediction accuracy.

Thus on a purely statistical basis, there is no detectable difference between the modelled results and the estimated static temperature. As the data used here were typical of the petroleum industry we are really saying that linear regression based curve-matching models for BHT recovery should not be applied to the majority of available commercial well data. This is problematic for several reasons, not least that commercial data comprises the vast majority of available crustal temperature measurements. Is it adequate to simply dismiss this data as incorrect and unrecoverable? At this point it should be remembered that, as demonstrated in Chapters 5 - 8, the statistics of regression do not reflect the accuracy of the predicted result but rather the uncertainty inherent within it. The statistics are not so much saying that the temperature prediction is either good or bad as how confident we may be in asserting either case. In this instance, however, there was an independent means of assessing the accuracy of the result. Observing the pattern of prediction from well to well it has been shown for most models that systematic variations are present. Were the statistics to be correct then all variation between the known and predicted temperature should be entirely random, a purely statistical error caused by uncontrollable data fluctuations. In reality, however, this is not the case. The deviation between modelled and actual formation temperatures instead appears to be a combination of both random scatter and systematic variation(s) that are dependent upon one or more model parameters. Situations like this, where an apparent result bias can be related directly to a systematic variation, are evidence of true model bias. The presence of such bias within these results implies that they should probably be considered meaningful.

Model	Stat1	Stat2	Systematic
Horner Plot	±4.5	±25	+2.1; -1.8
DMZC (Cooper & Jones, 1959)	±110	±516	+2.1; -1.5
Semi-log plot x = 20*t_C	±9.6	±30.5	+2.4; -2.3
Semi-log plot x = 50 hour	±6.3	±29	+2.0; -1.9
Exponential	-	-	+7.8; -2.2

Table 9.3: Estimated statistical and systematic uncertainties in temperature prediction for models of BHT temperature recovery. Stat1 = uncertainty calculated for linear regressions which pass the F-test for statistical significance at 95%. Stat2 = uncertainty calculated for linear regressions which do not pass the F-test at 95%. All results are presented as percentage of the actual predicted formation temperature. Note: the exponential solution does not involve linear regression.

There are several other lines of evidence which indicate that the temperature predictions, as calculated, may be more reliable than the statistics alone suggest. Firstly, there is the calculated systematic error, which in all cases is smaller than the statistical error. While it does not account for all possible random errors, the systematic error gives an indication of the size of the unavoidable empirical uncertainty. In this sense it is probably a minimum estimate of uncertainty in the regression. In all cases where linear regression is used, the average systematic error was calculated as less than ±3% (Table 9.3). For the two theoretical models this implies that the negative bias seen in Tables 9.1 and 9.2 is likely to be real. Secondly, the possibility that large random error could exist in this data should be reduced significantly by the data quality controls outlined in Chapter 4, an exercise that was designed to identify, isolate and remove large potential outliers from consideration. That this was relatively successful is evident in the high average R^2 achieved for each model. Any remaining outliers not eliminated during this process should have been removed by the practise of automatically eliminating model fits worse than $R^2 = 0.9$. Indeed, only two wells, the type 2 curves Ulandi 2 and Woolkina 2, were repeatedly identified as outliers to the main result populations.

It is probably not an unreasonable position then that the statistical uncertainty be considered to represent, in these instances, a worst-case scenario of uncertainty that is not actually realised. The results of the statistical analysis appear to be more strongly influenced by the small population size rather a lack of correlation in the data. That there are relatively few data points implies that the risk of random error is high for most regressions. It does not however imply that the random error actually is high. The fact is that input data quality was good, the extensive pre-modelling quality control process clearly successful in removing most rogue or outlying data points prior to modelling. As a consequence, both linear and non-linear regression correlations were strong and calculated systematic error was low. Compared to the possible range of statistical uncertainty, the actual result accuracy is relatively high and the effect of random error on temperature prediction is subordinate to systematic variations dependent upon one or more identifiable factors. In short, the observed influence of random error does not appear to be as great as would be suggested by the statistical uncertainty. As a result, the true reliability of model temperature predictions are assumed to be closer to the calculated systematic uncertainty than that of the statistical.

9.4 Comparing Model Results

It is probably inevitable that studies such as this, which test the performance of a number of parallel solutions to the same problem, should turn to the question of comparative behaviour. The issue of "which model performs best?" is significant to anyone planning to use these techniques in the future. To address this issue however it is necessary to first decide upon a definition of what 'best' is. Is the best model that which produces the most accurate mean result? or that of the most precise result? most reliable? or the easiest to produce? Is it a model whose behaviour is predictable? The answer, of course, is a mixture of all of the above and the leading model will be that which is judged to strike the optimal balance between each of these criteria.

In terms of the balance between accuracy and standard deviation the ideal model would appear to be the empirical semi-log plot at 50 hours. The success of this model may rest upon the fact that the chosen 50 hour extrapolation interval is close to twenty times the average duration of well circulation. This is, of course, within the range of time suggested by Bullard (1947) for full thermal equilibration. The semi-log plot also has the advantage of being an extremely basic model, requiring only a minimal number of input parameters, and is simple enough to solve manually. In many respects, this model seems to be the obvious candidate for 'top model'. There are a number of other considerations which must first be taken into account however, before making the final choice between theoretical and empirical corrections. Perhaps the most important of these are issues related to the predictability of model behaviour.

Model	**Initial t_L (hrs)**	**Total t_L (hrs)**	**Lag Window (hrs)**
Horner Plot	> 7	> 20	> 15
DMZC (Cooper & Jones, 1959)	> 7	> 20	> 15
Semi-log Plot	-	> 20	> 20
Exponential	-	> 30	> 25

Table 9.4: Empirical lag time control on prediction accuracy for various models applied to Cooper Basin well data. Well data which exceeds one of these lag time conditions should produce an unbiased temperature prediction within ±5% of the true formation temperature when corrected using the appropriate BHT recovery model.

The sensitivity analyses presented for the various models in Chapters 5 – 8 are uniform in at least one respect: for every model tested, the total length of elapsed lag time is found to exert a controlling influence on prediction accuracy. In each case it was possible to nominate a minimum value of total lag time which, if surpassed by the data, was sufficient to virtually guarantee prediction accuracy within around ±5% of the estimated static temperature (Table 9.4). Given the magnitude of the calculated systematic error it is likely that this precision is close to the true extent of random scatter in good data. For long lag time data, at least, it appears to matter little which model is employed as all appear to work to within roughly the same range of accuracy. Where the models differ, however, is in their respective behaviours at short lag times and significantly, in the length of total lag time required to produce unbiased temperature predictions.

The improvement of temperature prediction at increasingly long lag times across all models is a reasonable result. Longer lag times imply a more controlled data curve which in turn provides a greater control for the model fit. This commonality between the various model behaviours is underpinned by comparisons of their result populations (Figure 9.3). Here, despite some scatter, it is evident that there is some degree of correlation between virtually all of the tested models. No one model is behaving in an entirely random way relative to all the others, although perhaps the exponential model is more poorly behaved. Of particular note in this figure is the remarkably strong correlation between the results of the two theoretical models. This similarity was first mooted in Chapter 6 where it was observed that the pattern of control on the DMZC model of Cooper & Jones (1959) was remarkably similar to that generated by the Horner model. It is clear from Figure 9.3 that these models must be producing almost identical curve shapes. This is perhaps a little unexpected given the major differences in both theory and formulation between the two. It would seem that, despite the addition of significant complexity relative to the Horner model, the DMZC does not produce a better temperature prediction.

For both theoretical models it is apparent that short lag time data are systematically producing under-predicted formation temperatures. In the case of the Horner plot the causes of this behaviour are well established and are the combined result of the failure, at short lag times, of the assumption of a zero well diameter and the use of a curve-matching model (Chapters 3, 5; Figure 3.3). The almost identical behaviour of the DMZC model implies that something very similar must also be occurring. In this case this is most likely to be related to a failure, also at short lag times, of the assumption of zero circulation time. Unique to the theoretical models is an apparent condition of minimum initial lag time which, where exceeded by the data, appears to ensure unbiased prediction accuracies within around ±5% of the estimated static temperature. That there should be a lower limit to initial lag time is also consistent with the Horner model theory which stipulates a condition of minimum lag time for model validity (Chapter 5). For Cooper Basin wells this value appears to be around 7 hours, somewhat lower than was suggested by the initial estimates produced by equation (33) in Chapter 5.

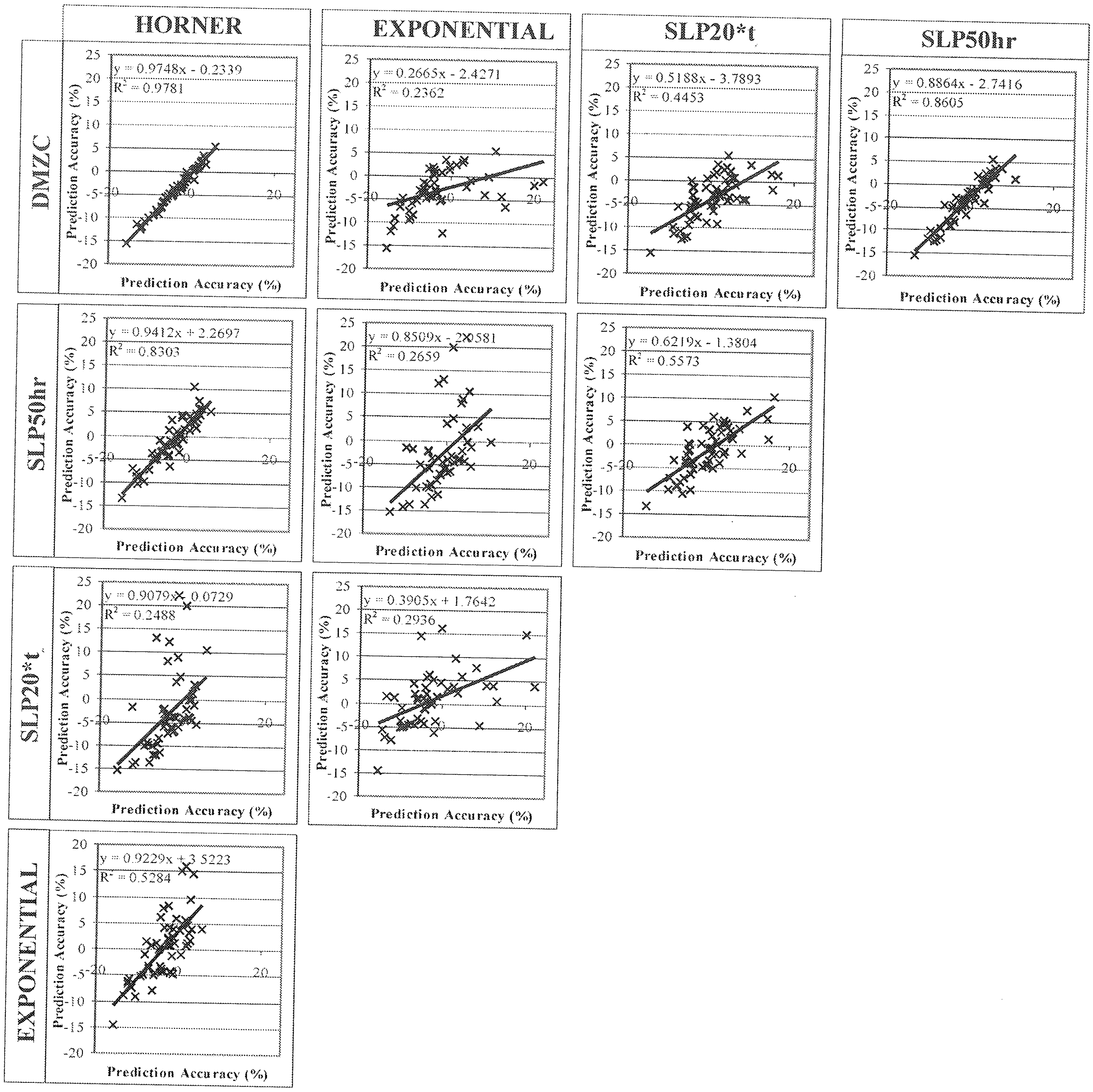

Figure 9.3: Comparative scatter graphs of formation temperature prediction accuracy relative to FTEX static temperatures from five models of bottom of hole thermal recovery. *x* and *y* axis labels are as given in top and side boxes.

Compared to the theoretical model results, temperature predictions based on short lag time data by empirical models show much less evidence of systematic bias. As a result the average prediction accuracy calculated for these models appears closer to the ideal than that of the theoretical model results. Temperature prediction by these models is dependent largely upon the attributes of the function when fitted to the data curve. In the semi-log plot this control is exercised by the gradient of the regression line whilst in the exponential model it is the concavity, expressed as the exponential constant α, which most influences prediction accuracy. In both cases increasing the total lag time improves the control of the model curve fit and consequently produces better results. At short lag times however, the qualities of the fitted model curve depend largely upon the sampled time window and the quality of the available data. In this case variations in these parameters were relatively random, a function of the data collection process in each well. As a result, the bias in individual empirical model temperature prediction at short lag times was also relatively random, producing a mean prediction accuracy that was closer to ideal. For a different set of well data, however, there could be no guarantee that these model results would be replicated. This is evidenced by the results of Hermanrud *et al.* (1990) (Table 3.1) for whom the exponential model behaved in such a way as to produce predictions that, while biased, were relatively precise.

Of the two types of models, theoretical and empirical, the solutions of choice would appear to be the Horner and semi-log plots. The former is preferred over the DMZC thanks to its simpler formulation and almost identical results. Also, contrasting strongly with the relative closeness of the accuracy of the predicted results generated by these two models is the vast increase in calculated statistical uncertainty associated with the DMZC (Table 9.3). From this perspective too, the Horner model is clearly a better choice. Between the two empirical models, the semi-log plot has the advantage in both mean prediction accuracy and precision (2σ). The flexibility of the exponential curve and its ability to fit the data almost perfectly in the majority of cases actually proves here to be a disadvantage, allowing a high number of outliers in cases where the number of available data points is low.

Between the Horner and SLP models the choice is less clear cut. Whilst the semi-log plot appears to have the advantage of prediction accuracy, it is subject to many questions about its reliability. For the majority of wells where total lag time is <20 hours, prediction appears to be related to random effects. Were this model to be applied to a different set of data there is no guarantee that the results would be the same or similar. By contrast, the physical nature of the Horner model implies that its behaviour should be more consistent. Comparison with the results of Hermanrud *et* *al.* (1990) support this conclusion. Hence, application of this model, even to data from another basin, should result in a similar pattern of prediction, albeit one which might be governed by different preferred lag time windows. This being the case, it is the Horner model that is considered to be the correction of choice for Cooper data, providing the wells in question meet the lag time requirements of Table 9.4. Although the Horner model requires an additional parameter in the form of circulation time, results from this study show that it is remarkably insensitive to this parameter. A best guess estimate should be adequate to ensure a reasonable result - providing of course that lag time conditions are met. In instances where this is not the case the Horner model will under-predict by some amount up to 20%. Under these circumstances it may perhaps be acceptable to substitute a semi-log plot extrapolation to 50 hours. For Cooper Basin wells, at least, results from this semi-log plot model to date are typically within around ±10% (2σ) of the true value, even at very short lag time.

9.5 Applications

Understanding the behaviour of models for BHT temperature correction is useful for a variety of real-world applications. Knowing the conditions under which a model may be expected to predict accurately implies it is possible to stipulate conditions both for the collection of new data as well as in the utilisation of existing records. Unfortunately at present, this can only be reliably done for Cooper Basin data, although the recommendations made here may be of some use as a qualitative guide for other areas.

9.5.1 Recommendations for Future Data Collection

One of the best features of the Horner model is that its theoretical grounding implies a degree of predictability in response. Using the results generated from this model it is possible to recommend that future Cooper Basin geothermal wells be drilled and evaluated such that the newly drilled wells be allowed to recover for a shift (twelve hours) prior to recording the first temperature measurement. On the basis of current results, wells left for this period and then logged at least three times (preferably four) will be corrected by the Horner model to within an unbiased 5% of the true formation temperature. This implies that it should be possible to obtain a reliable estimation of true formation temperature after a delay of only ten to twelve hours to the drilling program. Comparing this to the week to ten days that may be required to obtain a near-equilibrium bottom of hole temperature measurement for typical drilling times and the advantage becomes obvious.

9.5.2 The Corrected Cooper Temperature Map

The knowledge gained regarding the correction of perturbed borehole measurements in the Cooper Basin is also of great value in developing more accurate, reliable crustal temperature map. As discussed in Chapter 2 much of the data used in the 2003 Australian Crustal Temperature Map (Figure 2.17) was uncorrected, and hence perturbed, well BHT. Although the absolute value of constraints on the Horner plot are only established for Cooper Basin data, and therefore only BHT from this region may be corrected, it is still possible to use these data to examine the effects of employing corrected rather than uncorrected data in the production of a crustal temperature map. The presence of static or CBL temperatures from the Cooper Basin in the AUSTHERM03 database (Chapter 2) implies that, for this region, the image portrayed in the 2003 crustal temperature map is likely to be relatively reliable. To achieve a full comparison between the use of corrected and uncorrected BHT data in this area it was thus necessary to create two new temperature maps, one derived solely from data which displays the drilling induced perturbation, the other from model-derived static temperature estimations. The difference between these two images should provide an indication of the relative reliability of the many other areas on the 2003 map image for which no static temperature data were available.

The abundance of petroleum well temperature data available within the relatively small Cooper Basin region allowed a reasonably selective choice of wells for correction. Elimination of a number of points from this area was not likely to detract from the created map image because the high data density meant that many points were treated as duplicate by the original kriging process. Data for correction was selected on the basis of both the criteria set out in Chapter 4 and those defined above for unbiased correction by the Horner model. Each well selected for correction was characterised by:

1. At least three BHT with known lag times

2. A progressive increase in BHT with elapsed lag time
3. Depth separation of individual BHT from $z_{BHT} \leq |25m|$
4. No evidence of circulation between logging runs
5. An initial lag time >7 hours OR
6. A total lag time >20 hours OR
7. A window of lag time > 15 hours

A Horner Plot correction was applied to all selected wells using a standard three hour circulation time. A final round of eliminations was then made to remove all wells for which the fitted Horner regression line was characterised by an $R^2 < 0.90$. In total, 243 corrected BHT were retained for mapping along with a further 64 wells with known category 1 CBL BHT (Figure 9.4). The latter group included the 61 wells used in the previous modelling tests plus another three wells, Burley 2, Bulyeroo 1 and McLeod 1. Along with the coverage of 307 corrected and static temperature measurements a separate and otherwise identical coverage was created for the same points using the last available perturbed BHT measurement from each well. These two coverages, named Cooper_corrected and Cooper_uncorrected respectively formed the basis for two new crustal temperature maps.

Extrapolation of temperatures from depth of measurement to 5km depth was conducted for both corrected and uncorrected data using the same techniques and crustal models employed in Chapter 2. Generation of the Cooper corrected and uncorrected crustal temperature at 5km images was undertaken with the assistance of Dr Prame Chopra. Image processing was conducted in ArcInfo again using techniques identical to those described in Chapter 2 for the 2003 Australian Crustal Temperature Map. Initial attempts at interpolation produced maps that were dominated by edge-related image artefacts produced as a result of the relatively small surface area and irregular shape of the data coverage. To compensate for these effects a ring of 410 control points were selected from the AUSTHERM03 data coverage. These points were added to both the corrected and uncorrected coverages. All control points were located well outside the limits of the available Cooper data and none were included within the extent of the presented Cooper maps (Figure 9.5).

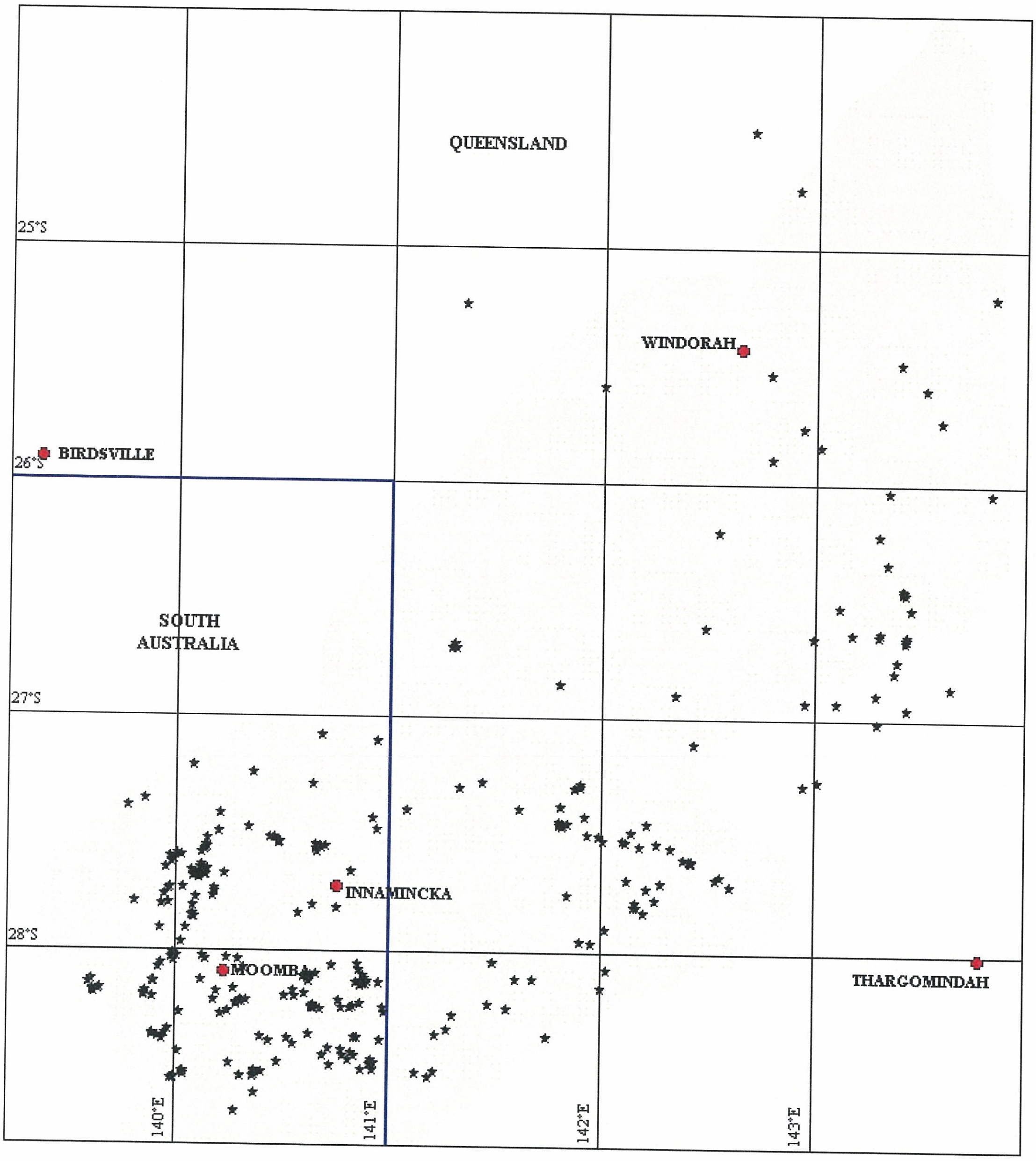

Figure 9.4: Location plan showing the 307 Cooper Basin wells with estimated static temperature. The shaded area indicates the interpreted extent of the Cooper Basin proper.

On average, the estimated temperature at 5km depth calculated from uncorrected data was around 10°C below that of the equivalent corrected data points. In all cases data from the Cooper_uncorrected coverage were lower than that from Cooper_corrected. A large range of temperature difference was apparent however, some uncorrected data points suppressed by only a few degrees, whilst others were up to 40°C below the corrected temperature. Although significant this is probably only a minimum estimate for the temperature perturbation that may be expected from using uncorrected BHT